Suppressing cyanobacterial dominance by UV-LED TiO2-photocatalysis in a drinking water reservoir: a mesocosm study.

PESTANA, C.J., SANTOS, A.A., CAPELO-NETO, J. et al.

2022

Water Research 226 (2022) 119299

Contents lists available at ScienceDirect

Water Research

journal homepage: www.elsevier.com/locate/watres

Suppressing cyanobacterial dominance by UV-LED TiO_2-photocatalysis in a drinking water reservoir: A mesocosm study

Carlos J. Pestana [a,1,*], Allan A. Santos [b,1], José Capelo-Neto [c], Vânia M.M. Melo [d], Kelly C. Reis [c], Samylla Oliveira [c], Ricardo Rogers [b], Ana B.F. Pacheco [b], Jianing Hui [e], Nathan C. Skillen [f], Mário U.G. Barros [g], Christine Edwards [a], Sandra M.F.O. Azevedo [b], Peter K.J. Robertson [f], John T.S. Irvine [e], Linda A. Lawton [a]

[a] School of Pharmacy and Life Sciences, Robert Gordon University, Aberdeen, UK
[b] Institute of Biophysics Carlos Chagas Filho, Federal University of Rio de Janeiro, Rio de Janeiro, Brazil
[c] Department of Hydraulic and Environmental Engineering, Federal University of Ceará, Fortaleza, Brazil
[d] Department of Biology, Federal University of Ceará, Fortaleza, Brazil
[e] School of Chemistry, University of St. Andrews, St. Andrews, UK
[f] School of Chemistry and Chemical Engineering, Queen's University Belfast, Belfast, UK
[g] Ceára Water Resources Management Company (COGERH), Fortaleza, Brazil

ARTICLE INFO

Keywords:
Phytoplankton
Advanced oxidation processes
Water quality
Microbial community
16S/18S rRNA sequencing
Mesocosm

ABSTRACT

Cyanobacteria and their toxic secondary metabolites present challenges for water treatment globally. In this study we have assessed TiO_2 immobilized onto recycled foamed glass beads by a facile calcination method, combined in treatment units with 365 nm UV-LEDs. The treatment system was deployed in mesocosms within a eutrophic Brazilian drinking water reservoir. The treatment units were deployed for 7 days and suppressed cyanobacterial abundance by 85% while at the same time enhancing other water quality parameters; turbidity and transparency improved by 40 and 81% respectively. Genomic analysis of the microbiota in the treated mesocosms revealed that the composition of the cyanobacterial community was affected and the abundance of *Bacteroidetes* and *Proteobacteria* increased during cyanobacterial suppression. The effect of the treatment on zooplankton and other eukaryotes was also monitored. The abundance of zooplankton decreased while *Chrysophyte* and *Alveolata* loadings increased. The results of this proof-of-concept study demonstrate the potential for full-scale, in-reservoir application of advanced oxidation processes as complementary water treatment processes.

1. Introduction

Climate change and anthropogenically-driven (hyper)eutrophication of surface drinking waters lead to an increase in frequency and severity of cyanobacterial mass occurrence events called blooms (Paerl and Huisman, 2008). Cyanobacterial blooms present significant challenges to the water treatment sector globally due to the potentially toxic cellular biomass in raw waters (Hitzfeld et al., 2000; Zamyadi et al., 2012). Modifying and upgrading existing infrastructure is often impractical and prohibitively costly. To counter the challenge posed by increased cyanobacterial blooms a paradigm shift to in-reservoir (pre--treatment) could be considered as an alternative treatment option. With targeted treatment of cyanobacteria and their toxins in the raw water prior to abstraction can ease the burden on existing water treatment plant (WTP) infrastructure. Promising technologies for in-reservoir pre-treatment include advanced oxidation processes (AOPs)(Camacho-Muñoz et al., 2020; Huang et al., 2011; Li et al., 2017; Menezes et al., 2021). AOPs are chemical processes that generate highly reactive oxidative species (radicals) that can remove organic contaminants. The application of chemical oxidants as algaecides (e.g. $KMnO_4$, H_2O_2, ClO_2) has been explored previously with limited success (Fan et al., 2014, 2013). Usually, biomass removal occurs upon the application of chemical oxidants, which is desirable, however, the reduction in cell density goes hand in hand with the release of intracellular cyanotoxins.

* Corresponding author.
E-mail address: c.pestana@rgu.ac.uk (C.J. Pestana).
[1] These authors contributed equally to this work.

https://doi.org/10.1016/j.watres.2022.119299
Received 10 June 2022; Received in revised form 21 October 2022; Accepted 23 October 2022
Available online 31 October 2022

A promising AOP for the removal of cyanobacterial cells and their toxins is semiconductor photocatalysis. TiO_2 is a semiconductor catalyst that upon incident of ultraviolet (UV) irradiation of <387 nm can generate hydroxyl ($\cdot OH^-$) and superoxide anion ($\cdot O_2^-$) radicals; via redox reactions on the surface of the photoexcited catalyst material in an aqueous matrix (Hoffmann et al., 1995). The removal of cyanobacteria and their toxins by TiO_2 nanoparticles has been previously documented (Lawton et al., 1999, 2003; Liu et al., 2003; Robertson et al., 1998a). The deployment of nano-particulate TiO_2-photocatalysis in water treatment plants , to date, has been limited by the lack of validation of bench-scale studies at pilot and industrial scale (Loeb et al., 2019). The main underlying factors of the limited pilot/full scale evaluation have been designing and testing of suitable photocatalytic treatment units that move the technology readiness level (TRL) up the scale. In the current study, we have made progress addressing the technology transfer from bench-scale testing towards implantation of the technology for water treatment by immobilizing TiO_2 nanoparticles onto beads made from foamed, recycled glass and using a low energy, waterproof UV-LED lighting system for deployment at mesocosm scale. In previous studies we have demonstrated the efficacy of the TiO_2-coated beads in controlling cyanobacteria and their toxins at bench scale (Gunaratne et al., 2020; Pestana et al., 2020c, 2020a) and at pilot scale (Menezes et al., 2021). This investigation evaluates the removal of cyanobacteria in a mesocosm study within an operating drinking water reservoir in the Northeast of Brazil that suffers from perennial cyanobacterial blooms. Our previous work, evaluation of H_2O_2 treatment of cyanobacteria, in this reservoir demonstrated the suitability of the constructed mesocosms and the study site to examine water treatment *in situ* (Santos et al., 2021). The current study sets out to evaluate:

- the efficiency of photocatalytic removal of cyanobacteria,
- the effect of treatment systems on physico-chemical water quality parameters,
- and the effect on non-target species of the microbial community

2. Material and methods

2.1. TiO_2-coated glass bead production and photocatalytic reactor construction

Glass beads made from foamed recycled glass (2-4 mm diameter; Dennert Poraver, Germany) were coated with TiO_2 according to a method described previously (Gunaratne et al., 2020; Pestana et al., 2020c). In short, acetone washed glass beads were repeatedly added to a TiO_2 slurry (0.1 g mL^{-1} P25 TiO_2 nanoparticulate powder [Degussa Evonik, Germany] in ultrapure water with 1 drop 5 mL^{-1} KD6 dispersant [Croda, UK]) and calcinated at 500 °C for 1 h until a w/w ratio of 10% TiO_2 was achieved (with each coating step depositing ~ 2% w/w), followed by a final calcination step at 500 °C for 10 h.

Coated beads were washed with ultrapure water to remove fines, dried at 100 °C, and stored until used.

The photocatalytic reactors were constructed from stainless-steel wire mesh with an aperture size of 1.2 × 1.2 mm and a wire thickness of 0.4 mm. The outer reactor consisted of a 1000 × 80 mm wire cylinder.

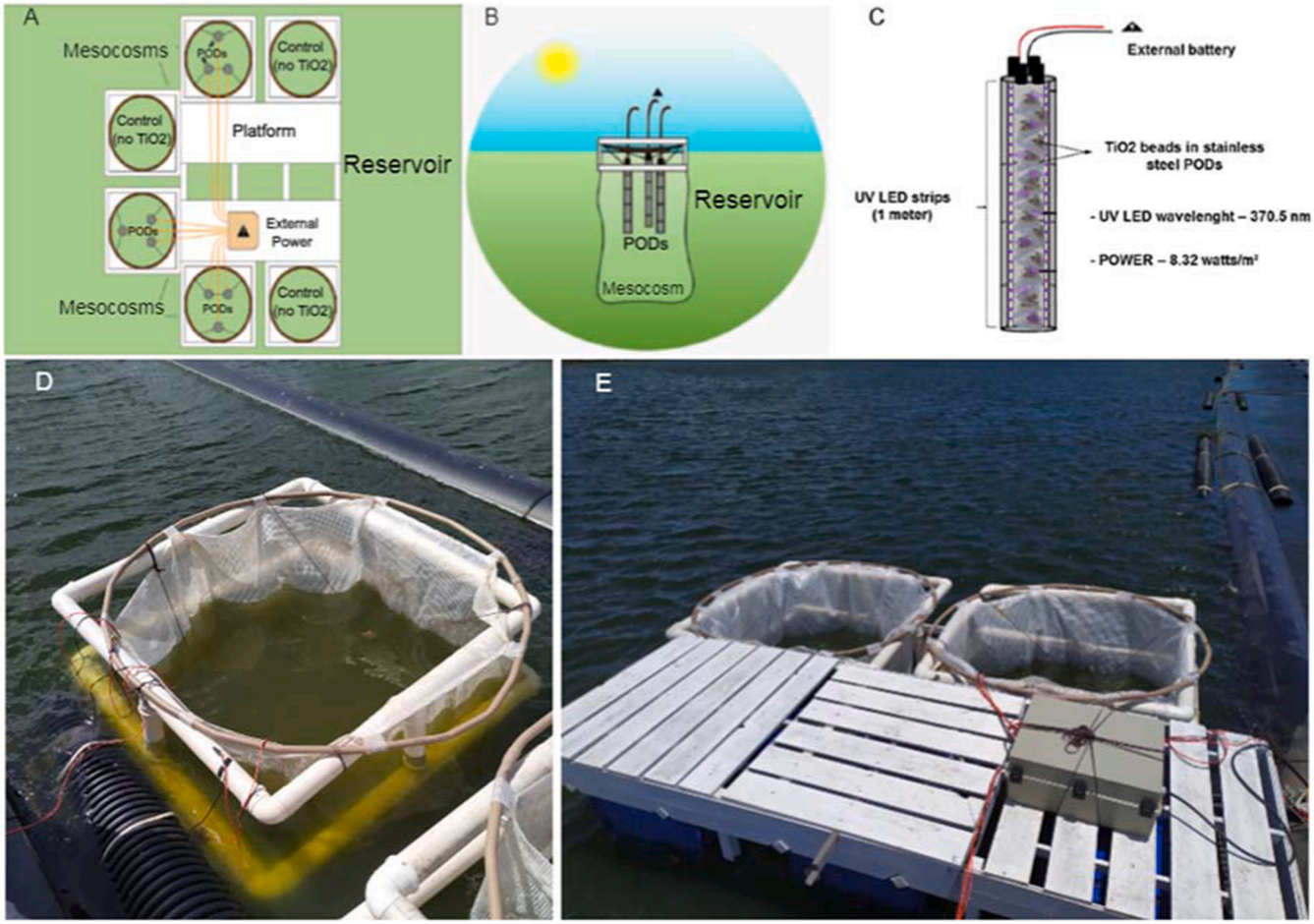

Fig. 1. Mesocosm deployment in Gavião reservoir October-November 2019. (A) Illustration of the platform containing three mesocosms for each condition (with and without TiO_2 reactors. (B) mesocosm with TiO_2-coated beads in stainless-steel pods. (C) Reactor design. (D) Mesocosm *in situ*. (E) Mesocosms with external power supply for LEDs.

Along the inside length of the mesh cylinder five aluminum profiles were attached with stainless-steel screws (Fig. 1c). Each profile housed a 1000 mm length of waterproof UV-LEDs (LightingWill, UK; 365-370 nm; IP68 rated, 4.8 W m^{-1}, 120 LEDs m^{-1}). Each set of five LED strips were powered by an AC/DC adapter that delivered 12 dcV and ~ 3A. The power output was 8.32 W m^{-2} on average. Tetrahedral wire mesh pods (18; made from the same wire mesh as the outer reactor) containing 8 g of TiO_2-coated glass beads each were placed inside the wire mesh cylinder. Reactors were capped, top and bottom, with 80 mm diameter wire mesh disks. Waterproof connectors were used to supply a mains power line which was run from onshore.

2.2. Experimental site and mesocosm set-up

The current study was conducted in the Gavião Reservoir (3°59'03''S/38°37'13''W), a drinking water system located in a semi-arid area in the Northeast of Brazil; that presents a high solar radiation reaching about 5 kWh m^{-2} day^{-1}, 8 h per day, and an average atmospheric temperature of 32 °C (FUNCEME, 2017; Barros et al., 2019). Gavião Reservoir is known for perennial cyanobacterial blooms (Barros et al., 2019). In general, the is eutrophic, presenting an average depth of 10 m in the lacustrine zone, with a water storage capacity of 3.3×10^7 m^3 in a hydraulic basin of 618 hectares and a water retention time of about 22 days on average (Barros et al., 2019; Santos et al., 2021). The study was carried out in October-November 2019 with an average air temperature of 28 °C (maximum: 32 °C), and < 0.1 mm precipitation according to the National Institute of Meteorology - INMET (INMET - National Institute of Meteorology (Brazil), 2019; Table S1). Six mesocosms were constructed, consisting of a cylindrically shaped bag (1.5 m diameter and 2 m depth) of impermeable and semi-transparent plastic which was supported and kept afloat by a PVC (polyvinyl chloride) tube structure. The mesocosms were tethered to a floating platform which housed the electronic components for the photocatalytic reactors, located close to the WTP intake point. The bottom of the mesocosm was completely sealed, separating the water inside from the reservoir (Fig. 1). All mesocosms were filled with approximately 3000 L of reservoir water. The controls were tree mesocosms with no photocatalysis and three which housed the LED-powered-TiO_2 reactors (Fig. 1).

2.3. Sampling and monitoring analyses

For each sampling time (0, 3 and 7 days), abiotic and biotic parameters were analyzed (Table S2). Composite samples were collected with a 1800 × 50 mm long PVC pipe and tight-fitting rubber bung by placing the pipe in the center of the mesocosm and submerging it the entire depth of the mesocosm; it was then capped with the rubber bung and the sample was removed and placed into amber glass bottles that were stored at 4 °C until laboratory analysis. To obtain the microbial community, 500 mL of water was filtered through 0.22 μm SteritopTM filter units (Merck Millipore®, Massachusetts, US). The material retained on the filters was used for DNA extraction.

2.4. DNA extraction, amplification and high-throughput sequencing

Membrane filters containing cells were cut into pieces with sterile surgical blades and used to extract DNA with the cetyl trimethylammonium bromide (CTAB)-based method, that uses a cationic detergent to disrupt cells. The procedure was performed according to Winnepenninckx et al. (1993). The concentration and quality of DNA preparations were verified with a Nanodrop ND-1000 spectrophotometer (Thermo Scientific, Waltham, MA, USA). The V4 region of the 16S rRNA gene and the V9 region of the 18S rRNA gene were targeted to determine the composition of the bacterial and eukaryotic plankton communities. The respective set of primers was 515F/806R (F515 - 5′ GTGCCAGCMGCCGCGGTAA 3′ and R806 - 5′ GGACTACHVGGGTWTCTAAT 3′) for Bacteria (Caporaso et al., 2011) and Euk1391f/EukBr (Euk 1391f - 5' TATCGCCGTTCGGTACACACCGCCCGTC 3') and EukBr - 5' AGTCAGTCAGCATGATCCTTCTGCAGGTTCACCTAC 3') for Eukarya (Amaral-Zettler et al., 2009). The first amplification, incorporating barcodes in the forward primer, was performed using the following program: 95 °C for 4 min, 60 °C for 1 min, 72 °C for 2 min, followed by 25 cycles at 94 °C for 1 min, 60 °C for 1 min, and 72 °C for 2 min. Each sample was marked with a specific barcode so that it could be recognized after high-throughput sequencing. The resulting amplicons were purified using calibrated Ampure XP beads (Beckman Coulter, Indianapolis, IN, USA) according to the manufacturer's instructions. All samples were subjected to a second PCR to incorporate dual indices as described in the 16S and 18S Metagenomic Sequencing Library Preparation Protocol for the Illumina MiSeq system (San Diego, California, US). Final amplicons were paired-end sequenced using an Illumina MiSeq Reagent Kit v2 (500 cycles, 2 × 250 bp) on an Illumina MiSeq sequencer (Illumina, San Diego, CA, USA).

2.5. Data acquisition and processing

After sequencing, Illumina adapter sequences were trimmed from already-demultiplexed raw fastq files using Cutadapt v1.8 (Martin, 2011) in paired-end mode, and the reads quality were assessed using FastQC v.0.11.8 (Andrews, 2010) and vsearch v2.10.4 (Rognes et al., 2016). Subsequent analyses were performed in the R v3.5.3 environment (R Core Team, 2020), following the DADA2 v1.11.1 package (Callahan et al., 2016) pipeline to obtain a table of non-chimeric amplicon sequence variants (ASVs; sequences differing by as little as one nucleotide) (Callahan et al., 2017). Taxonomy assignment and removal of non-bacterial sequences was performed against the SILVA reference database (release 138, December 2019) (Callahan, 2018; Yilmaz et al., 2014), whereas the assignment for eukaryotic community was performed using the PR2 reference database (Guillou et al., 2013). The 16S and 18S rRNA data were deposited in the NCBI Bioproject database with accession no. PRJNA754369 and PRJNA754602, respectively (https://www.ncbi.nlm.nih.gov/bioproject).

2.6. Statistical analysis

For a detailed description of the statistical analysis please refer to the supplementary material (S2.2). In short, for the abiotic factors principal component analysis (PCA) followed by Shapiro-Wilk determination ($p<0.05$) and a Wilcoxon-Mann-Whitney test to determine significant differences in relevant parameters between treatment and control was carried out. Statistical analyses for abiotic factors were performed using R software version 3.4.1, using the Factoshiny package (Vaissie et al., 2020).

For biotic factors (bacterial and eukaryotic plankton communities), we performed a linear discriminant analysis (LDA) and effect Size (LEfSe) (Segata et al., 2011) (the Hutlab Galaxy web framework - http://huttenhower.sph.harvard.edu/galaxy/) to select significant biomarker taxa ($p<0.05$) between treatment and control over time (at genus level) using LDA score of 3.5 as threshold (log_{10} transformed).

From the 18S rRNA data, we used the taxonomic groups identified and gathered the main taxa (>3% relative abundance in at least one sample) in relevant freshwater plankton groups, following the classification described in previous studies (Cavalier-Smith, 2018; Simpson and Eglit, 2016; Table S2). The beta-diversity ordination was evaluated by nMDS (non-metric dimensional scaling) considering ASVs abundance in a tridimensional space using the Bray-Curtis distance as dissimilarity matrix, which was complemented by permutational multivariate analysis of variance (two-way PERMANOVA) using two factor groups, condition (control and treatment) and time ($p<0.05$). To test the correlation between abiotic and biotic (ASVs-based taxa) factors and differences in the community structure over time, the samples were ordained by Canonical Correspondence Analysis (CCA) using the Hellinger-transformed

abundance matrix and Spearman analysis ($p<0.05$ and a threshold for r value $=\pm 0.4$). The analyses were performed, and charts plotted in R v3.5.3 environment (R Core Team, 2020) and Past3 software (Hammer et al., 2001).

3. Results and discussion

3.1. Effect of TiO_2 photocatalysis on cyanobacteria and raw water quality

The TiO_2-based photocatalysis treatment system placed in mesocosms in a eutrophic reservoir in Brazil significantly affected bacterioplankton dynamics when compared to the control ($p=0.001$ $F=3.90$) over time ($p=0.0001$ $F=8.25$) according to PERMANOVA analysis. nMDS ordination provides a clear distribution opposing control and treatment conditions, mainly for the day 7 (Fig. S1).

Following treatment using TiO_2 photocatalysis the relative abundance of the cyanobacteria decreased in the treatment mesocosms compared to the control mesocosms (Fig. 2).

Initially, the bacterioplankton composition was dominated by *Cyanobacteria*, with 45% relative abundance on average, and members of *Bacteroidetes, Verrucomicrobia, Planctomycetes* and *Proteobacteria* contributed as major other phyla (Fig. 2B). After three days, the relative abundance of cyanobacteria decreased to about 33-35% (Fig. 2 and Table S3). The most pronounced effect of the treatment was observed on day 7, when the cyanobacterial contribution decreased to less than 5%, on average, in the mesocosms where the photocatalytic units had been deployed, while it represented approximately 25% in the control. This selective removal of cyanobacteria by ROS-based treatment methods has been described previously and is linked to the internal structure of cyanobacteria and the co-action of irradiation-induced intracellular ROS generation (Drábková et al., 2007). Specifically, the photosynthetic apparatus in cyanobacteria is not segregated into organelles and has direct connection with the plasma membrane of the cell, thus making it more susceptible to ROS attack (Grossman et al., 1995) and the cyanobacterial light-harvesting complex (the phycobilisome) is located outside of the thylakoidal membrane thus, making it more susceptible to external ROS attack (Grossman et al., 1995). Cyanobacteria have also been shown to be sensitive to ROS attack due to having a limited enzymatic defense mechanism lacking the common ROS-eliminating ascorbate peroxidase (Passardi et al., 2007) and most species further lacking alternative members of the haem peroxidase family of ROS-defense enzymes (Bernroitner et al., 2009). Further, it has been shown that irradiation-induced intercellular generation of ROS by the Mehler reaction can overwhelm the internal enzymatic ROS defense mechanisms under increased irradiation levels such a those presented by the UV-irradiation provided by the photocatalytic reactors in the current study (Tytler et al., 1984). Additionally, it has been demonstrated that the phycocyanin pigment, which is unique to cyanobacteria, can

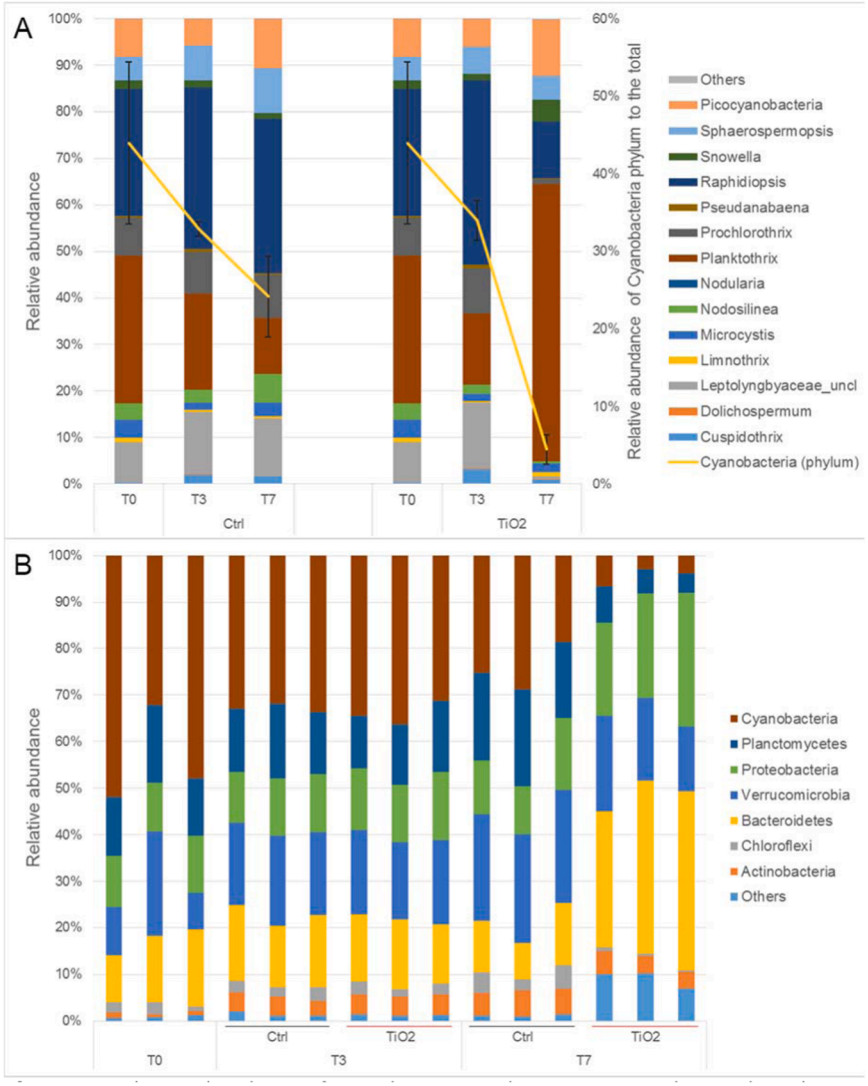

Fig. 2. Relative abundance of cyanobacteria in the treatment and control condition over time determined by 16S rRNA sequencing (A) and dynamics in the relative abundance of the phyla in the bacterioplankton over time also determined by 16S rRNA sequencing (B). In (A), the secondary axis shows the relative abundance of the cyanobacteria phylum in relation to the entire bacterioplankton community (yellow line, grouping the mean and standard deviation). The bars resulted from triplicate samples (n=3). In (B) the effect of TiO_2-based photocatalysis (red TiO_2) on the main phyla of the bacterioplankton community compared to the untreated control (black Ctrl) is shown. Data from triplicate samples for both conditions (n=3). Taxa designated as "others" are described in Table S4.

enhance photocatalytically-generated ROS attacks (Robertson et al., 1998b). The combination of these effects is responsible for the selective sensitivity of cyanobacteria to the proposed treatment system. *Planctomycetes* abundance also decreased following photocatalytic treatment compared to controls. In contrast, *Bacteroidetes* increased its abundance from 14% in the control to 35%, on average, following photocatalytic treatment and *Proteobacteria* increased in abundance from 12% in the control condition to 24% with photocatalytic treatment (Fig. 2 and Table S3).

Using different loadings of TiO_2 nanoparticles (15, 100, and 1000 mg L^{-1}) in samples from three different Swedish lakes, Farkas et al. (2015) observed a high impact on the bacterial community in a dose dependent manner, considering their abundance and activity, which was estimated by the incorporation of radioactive labeled L-[4,5-^{3}H]-leucine. They also reported that the light regime considering the UV and PAR (photosynthetically active radiation) sources compared to the dark condition contributed to the decrease on bacterial activity mainly from the highest concentration of TiO_2 nanoparticles. Moreover, the authors observed that TiO_2 effects on bacterial abundance and activity were stronger in lakes with high dissolved organic carbon (DOC) and low chemical

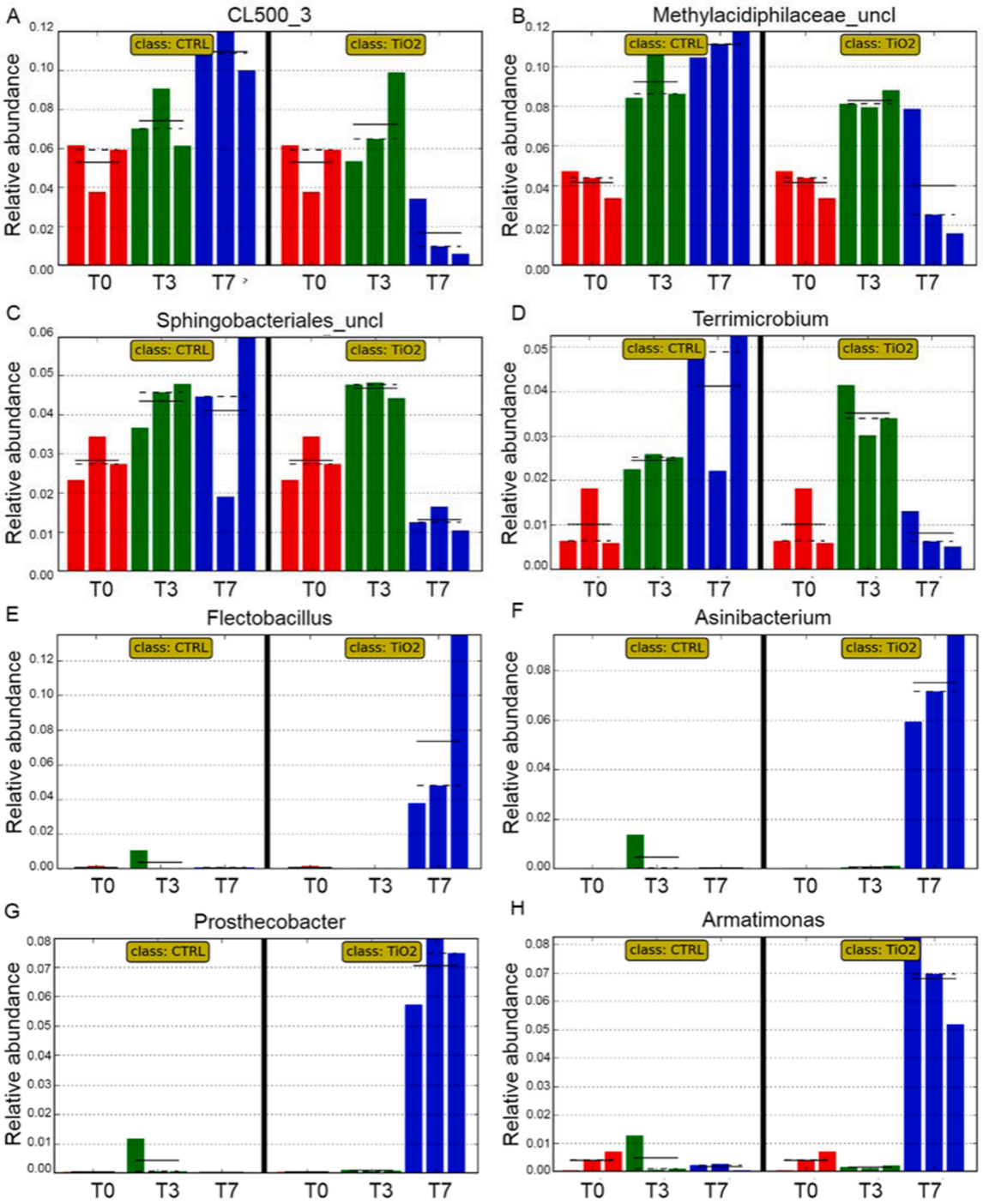

Fig. 3. Differential abundance of heterotrophic bacterial taxa affected by TiO_2 compared to the control condition according to LEfSe analysis ($p < 0.05$), considering sensitive (A–D) and resistant organisms (E–H). The different colors express the sampling days T0 (red), T3 (green) and T7 (blue) from the triplicate samples. Full black lines represent the average of three samples, the dashed black line represents the median.

elements concentrations; however, they did not investigate any modification on bacterioplankton composition.

In our findings, LEfSe analysis identified the most important taxa considering cyanobacteria and non-cyanobacteria that contributed to the differential abundance between treatment and control ($p < 0.05$) (Fig. S2). Using a LDA threshold of 3.5, we selected 38 genera that reflected the effect of TiO_2 on the 7th day, including 18 resistant and 20 susceptible taxa.

We observed that the main susceptible organisms, besides cyanobacteria, were unclassified taxa from *Phycisphaeraceae* (CL500_3), and *Methylacidiphilaceae* families, *Sphingobacteriales* order as well as the genus *Terrimicrobium* compared to the control condition (Fig. 3A–D). The resistant taxa, *Flectobacillus, Asinibacterium, Prosthecobacter* and *Armatimonas* contributed to about 60% of the bacterioplankton community in the treatment mesocosms (Fig. 3E–H).

The application of TiO_2 photocatalysis represents a continuous low-level treatment with a steady production of reactive oxigen species (ROS) compared to the addition of oxidants (e.g., hydrogen peroxide) that are dosed at a set concentration with an (almost) immediate, albeit short-lived effect. This is clearly demonstrated when comparing our previous study (Santos et al., 2021) investigating the application of hydrogen peroxide in mesocosms to the current one. In this study, photocatalytic treatment showed a marked decrease in the cyanobacterial phytoplankton portion between days 3 and 7 of the treatment compared to a marked decrease for cyanobacteria after 24 h for the hydrogen peroxide study conducted in the same reservoir. Apart from *Cyanobacteria*, other susceptible taxa were identified as heterotrophic members of the *Phycisphaeraceae* family (*Planctomycetes*), this appears reasonable as this family has been described as directly related with cyanobacterial taxa in marine (*Synechococcus*) and freshwater systems (*Microcystis*) (Chun et al., 2019; Zheng et al., 2020), explaining their simultaneous decrease in relative abundance (Fig. 3).

Additionally, *Terrimicrobium* (*Terrimicrobiaceae*) identified in the current study as susceptible to the treatment process was also identified as vulnerable after H_2O_2 treatment in this same reservoir (Santos et al., 2021).

Flectobacillus, Asinibacterium, Prosthecobacter and *Armatimonas* were identified as resistant taxa in the current study (Fig. 3E–H) increasing in relative abundance as the cyanobacterial (and other susceptible taxa) abundance decreased in the treatment mesocosms.

Reasons for resistance against ROS attack could be an increased production of carotenoids, as observed by Asker et al. (2012) for *Flectobacillus* in a radioactively impacted region in Japan. Asker et al. (2012) and others (Martínez-Laborda et al., 1990; Stafsnes et al., 2010) proposed that carotenoids were able to quench ROS produced by UV-irradiation and photo-oxidation. Besides the production of pigments such as high carotenoid contents, the protection against ROS may be due to the efficient enzymatic activities for reducing the oxidative damage (Slade and Radman, 2011; Takebe et al., 2007). The resistance/tolerance to ROS-attack allows taxa to capitalize on resource availability or reduced competition (Litchman et al., 2015) explaining the marked increase of the aforementioned resistant taxa in the treatment mesocosms.

As mentioned earlier, *Cyanobacteria* dominated both bacterioplankton and phytoplankton which was also observed by other authors for the same and similar reservoirs (Dokulil and Teubner, 2000; Guedes et al., 2018; Liu et al., 2019). Focusing on the genus level, 40 genera were observed consisting of *Cyanobacteria* (18), *Chlorophyta* (11), *Bacillariophyta* (5), *Charophyta* (3), *Euglenozoa* (2), *Cryptophyta* (1) and *Ochrophyta* (1) (Table S6). *Cyanobacteria* reached approximately 98% of the total phytoplankton with a density of around 10^6 cell mL^{-1} in both control and treatment conditions. The composition of the observed cyanobacteria genera, originally composed mainly of *Planktothrix agardhii, Raphidiopsis raciborskii, Pseudoanabaena sp.* and *Pseudolyngbya sp.*, was modified by the treatment. Within the cyanobacteria grouping, a dominance of *Planktothrix* and *Raphidiopsis* in the original community (32% and 28%, respectively) (Fig. 2A) was observed. Additionally, <10% Picocyanobacteria (including *Cyanobium, Synechococcus* and *Synechocystis*), *Sphaeropermopsis, Prochlorothrix, Microcystis* and an unclassified genus of *Leptolyngbyaceae* (Fig. 2A) were detected.

On day 3 of the experiment, *Raphidiopsis* presented a higher abundance than at T0 while *Planktothrix* decreased in abundance in both conditions. Following the decrease of cyanobacterial abundance by the 7th day, *Planktothrix* (61%) presented the highest relative contribution of cyanobacteria compared to the other sampling times and to the control. We also detected a higher resistance of *Planktothrix* compared to the other *Cyanobacteria* genera (Fig. 2A). Santos et al. (2021) monitored cyanobacteria by pigment fluorescence and the bacterioplankton composition (16S rRNA sequencing) after applying 10 mg L^{-1} H_2O_2 to a mesocosm system in the same drinking water reservoir. *Cyanobacteria*, originally composed of *Planktothrix sp.*, *Raphidiopsis sp.*, *Microcystis sp.* and *Cyanobium sp.*, were suppressed for 5 days after a single application of H_2O_2. Non-filamentous cyanobacteria were most resistant against H_2O_2, while *Planktothrix* sp. was markedly affected throughout the treatment; interestingly unlike the results presented here. Thus, in both mesocosm studies *Planktothrix* sp. and *Raphidiopsis* sp. dominated the initial cyanobacterial community but although both H_2O_2 and TiO_2/UV produce ROS, they affected the cyanobacterial community differently.

However, there is no clear evidence that supports different pattern of interspecific resistance/sensitivity, mainly for *Raphidiopsis* sp. and *Planktothrix* sp. considering specific ROS. For treatment purposes this aspect should be further explored since both cyanobacterial genera have shown a co-dominance (along with *Dolichospermum* sp.) in drinking water reservoirs, mainly in the Brazilian semi-arid region (Barros et al., 2019; Clemente et al., 2020; Pestana et al., 2019; Santos et al., 2021). Interestingly, in H_2O_2 studies at lab scale, (Yang et al., 2018) evidenced similar values for effective concentration (EC_{50}) of H_2O_2 that inhibit the growth of *Planktothrix* (0.42 mg L^{-1}) and *Raphidiopsis* (0.32 mg L^{-1}) as well as damage to the photosynthetic apparatus, whereas non-filamentous *Microcystis* presented higher resistance.

The diverse composition of other cyanobacterial taxa and the bacterioplankton community in each case may have affected the different outcomes in terms of competitive or synergistic interactions and succession.

More detailed information on the genomics data is provided in the Supplementary Information (Figs. S2 and S3, as well as Tables S4 and S5).

Physico-chemical parameters representing water quality markedly improved over the course of the study in the treated mesocosms versus

Table 1
Effect of TiO_2-based photocatalysis on selected water quality parameters in mesocosms located within a drinking water reservoir. Data from triplicate samples for both conditions.

Parameters	Raw water (T0)	3 days		7 days	
		Treated	Control	Treated	Control
Transparency (cm)	51 ± 2.7	96 ± 3	52 ± 5	96 ±18	53 ± 3
Turbidity (TU)	6.76 ± 0.25	3.83 ± 0.42	6.04 ± 0.18	2.37 ± 0.77	4 ± 0.52
True Colour (HU)	69.5 ± 6.6	68.2 ± 10.9	72.1 ± 7.8	98.3 ± 44.6	85.8 ± 14.2
pH	8.85 ± 0.16	9.63 ± 0.17	9.73 ± 0.21	8.22 ± 0.13	8.61 ± 0.12
Organic Matter (UV_{254nm})	0.261 ± 0.01	0.252 ± 0.01	0.261 ± 0.01	0.261 ± 0.02	0.261 ± 0.01
Total Organic Carbon (mg L^{-1})	21.57 ± 3.07	17.73 ± 0.85	21.57 ± 1.91	15.27 ± 0.38	18.33 ± 0.93
Dissolved Organic Carbon (mg L^{-1})	14.57 ± 1.16	16.63 ± 0.91	16.8 ± 3.07	14.4 ± 0.72	17.07 ± 1.46
Dissolved oxygen (mg L^{-1})	7.32 ±1.53	3.21 ± 1.13	6.17 ± 0.19	3.07 ± 1.19	6.17 ± 0.1

the control mesocosms (Table 1).

Transparency almost doubled on average in the treatment mesocosms, while turbidity practically halved, which is logical as both parameters are inversely related. This observation was confirmed by PCA analysis which identified pH, total and dissolved organic carbon (TOC and DOC), dissolved oxygen, turbidity, and transparency as the most relevant physico-chemical variables (Fig. S3). The pH was directly proportional to the variables TOC and DOC. The highest values of transparency were associated with the lowest values of turbidity and dissolved oxygen.

This trend for turbidity and transparency was also observed in our previous study with solar irradiation and hydrogen peroxide (10 mg L^{-1}) applied in the same reservoir (Santos et al., 2021). Increased transparency represents an improvement in the water quality both for treatment purposes and from an ecological perspective. The fact that the TiO_2-photocatalysis applied here reduced the turbidity and increased the transparency means it improved its own performances for the treatment purposes. Its effective capability for these physical aspects should be emphasized sinceorganic particles initially competed with bacteria for ROS and for the photoactive sites of the TiO_2. Furthermore, suspended particles reduced light penetration through the water by dispersion. By reducing these effects, the treatment became more effective, which could be a possible explanation for the lag time in observable effects of the treatment on the phytoplankton communities before day 7. Ecologically, greater transparency means light can penetrate deeper into the water column thus expanding the euphotic zone and generating oxygen in deeper zone of the reservoir. Additionally, eukaryotic phytoplankton can take better advantage of light penetration growing faster and bringing new stability to the water system.

A reduction of the dissolved oxygen concentration was observed throughout the experiment, which may have been caused by two mechanisms: the action of the oxidative process promoted in the treatment reactors and the water retention inside the mesocosms. The latter reduces the mixing processes of the water column, thus influencing its stratification (Båmstedt and Larsson, 2018). The depth of the mesocosms in the current study (1.5 m), is comparable to shallow areas within reservoirs or reservoirs that experience water shortage and are only fractionally filled. This, combined with the fact that the experiment took place during the time of year with traditionally high temperatures, the current mesocosm design could favor weak thermal stratification inside the system comparable to most reservoirs in the Brazilian semi-arid region (Marques et al., 2019).

Regarding the DOC concentration, values remained close to the control at T0 and day 3 with no major changes observed. The concentrations of TOC followed a similar trend as that observed for DOC. TOC results showed little significant differences in most experimental times after exposure to the photocatalysis.

There was no modification of nutrient or salt ion concentrations over time, as would be expected (supplementary information S4, Table S6, Fig. S4). The continuing presence of nutrients could theoretically favor regrowth of the cyanobacteria, which is why it is important to bear in mind that the current system is designed to be continually operating and treating the reservoir, it is not designed to prevent the formation of blooms by nutrient-control, but by population-control.

3.2. Effect of TiO_2 photocatalysis on the eukaryotic plankton community

Combined with the marked effects on the bacterioplankton community in the reservoir the TiO_2/UV treatment significantly affected the eukaryotic plankton community in general ($p=0.0049$ $F=3.21$ according to PERMANOVA when compared to the control) over time ($p=0.0001$ $F=6.73$), especially for the zooplankton community. nMDS ordination provides a clear distribution opposing control and treatment conditions, mainly for the day 7 (Fig. S1). While little change was observed at day 3, on day 7 of the treatment the zooplankton community decreased from around 61% of the total eukaryotic plankton community to less than 5% (Fig. 4).

Originally, the community was rich in zooplankton, followed by the diatom and alveolate groups, which together accounted for over 75% of the eukaryotic plankton community (Fig. 4). The *Arthropoda* subclass *Copepoda* was the main component of zooplankton, accounting for 50% on average (Table S7), with *Calanoida* and *Cyclopoida* as the main taxa in this group (Table S3). Diatoms contributed ~13% of the total eukaryotic plankton community including *Fragilariales* as the major group (10% of Diatom). Alveolate represented ~6% of the total eukaryotic plankton community with *Dinoflagellata* as the main representative (4% of Alveolate) (Fig. 4, Table S7). On day 3, there was no clear evidence of compositional changes except for an increase in the abundance of an unclassified member of Eukarya and a decrease in the diatom group (to 7% on average), although this occurred in both conditions (Fig. 4 and Table S7).

On day 7 the relative abundance of zooplankton decreased by more than 95% on average (Fig. 4 and Table S7) whereas *Chrysophyte* increased to about 41% compared to its low abundance at the start of the experiment and in the control condition on day 7 (0.5%-1%). The decrease in the relative abundance of zooplankton components may be a direct effect of the oxidizing treatment or a secondary effect due to changes in the phytoplankton community composition, mainly linked to the modification of cyanobacterial dynamics where *Planktothrix* dominated the cyanobacteria community compared to the original distribution at T0 and the control condition, where *Raphidiopsis, Pseudoanabaena* and *Pseudolyngbya* were more prevalent (Fig. 2A). Different zooplankton species have different preferred target food species (Tõnno et al., 2016); however, it stands to reason that in a biome that is so strongly dominated by cyanobacteria as is the current study site, a large portion of the zooplankton grazes on cyanobacteria as preferred food source. Thus, a possible explanation of the marked decrease of the zooplankton abundancy is that due to the reduction of cyanobacterial abundance an important food-source for zooplankton was removed leading to the zooplankton reduction. A detailed investigation of the zooplankton species present in the reservoir and an investigation of their feeding behavior would clarify these possibilities but was out with the scope of the current study.

Within *Chrysophyte*, the taxa *Chromulinales* (12%), *Chrysophyceae* (10%) and *Ochromonadales* (19%) family/order presented the highest increase in contribution (Table S6), suggesting resistance to the treatment. Interestingly, the *Chrysophyte* also referred to as golden-brown algae, presented an increase in the treated mesocosms which is unlikely as was observed for the effect of H_2O_2 in different studies; where the treatment promoted the growth of green algae when applied to mitigate cyanobacterial blooms (Fan et al., 2019; Santos et al., 2021; Yang et al., 2018).

An unclassified member of Eukarya increased to 22% in the treatment compared to < 5% in the control condition. Although less abundant, alveolate also increased in abundance at this time. Members of the family *Perkinsidae* reached about 8% of relative contribution compared to T0 or the control condition (~1%) (Table S7).

Following this pronounced modification on day 7, LEfSe analysis identified the most important eukaryote taxa contributing to the observed effect ($p < 0.05$) (Fig. S2B). Using the LDA 3.5 threshold, we detected a lower number of taxa that distinguished the TiO_2 based photocatalysis treatment and the control condition, where resistant and susceptible components included 11 and 8 taxa, respectively.

Besides *Calanoida* and *Cyclopoida* organisms, we observed the zooplankton *Ploimida* (*Rotifera*) and the fungi *Catenaria* (*Blastocladyales*) as susceptible organisms (Fig. 5A–D). These four taxa represented about 60% of the original eukaryote community, which was considerably diminished on day 7.

In the resistant group, with the highest LDA scores in the TiO_2 treatment, we identified *Ochromonas* (*Ochrophyta*), *Chrysophyceae_uncl* (unclassified), *Poteriospumella* (*Chrysophyte*) and *Nuclearia* (*Gastrotricha*) (Figs. 5E–H and S2B). *Ochromonas, Poteriospumella* and *Nuclearia* did not

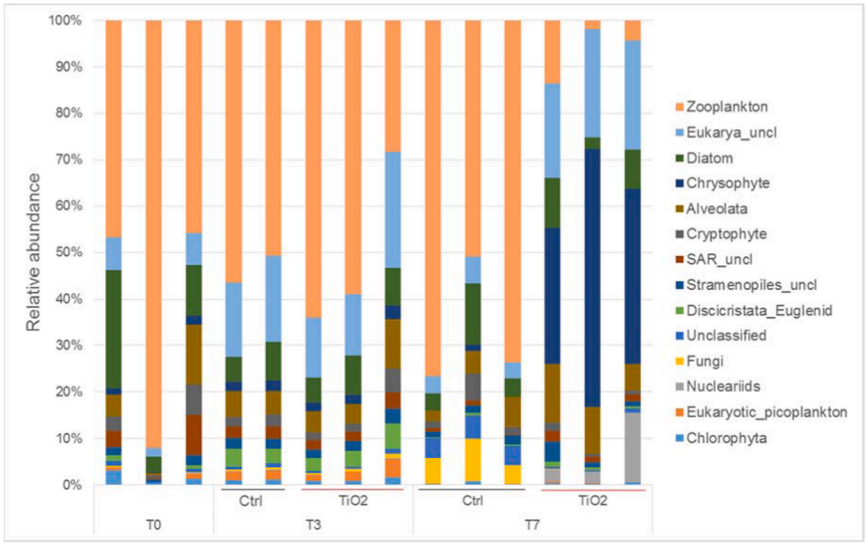

Fig. 4. Effect of TiO_2-based photocatalysis on eukaryotic plankton community showing the taxonomic composition with the relative abundance of the main planktonic groups. The main taxa identified after sequencing (>3% of relative abundance in at least one sample) were grouped in relevant freshwater planktonic groups. Data from triplicate samples for both conditions (n=3), except for the control condition at day 3, in which one replicate was removed due to the low number of sequences recovered.

present significant abundance at any sampling time, except for day 7 of the treatment condition, when their abundances rose to 15% and 6-7%, respectively, indicating a resistance to the TiO_2-based photocatalysis (Fig. 5E, G and H, respectively).

Following that, *Poteriospumella* and *Ochromonas* genera from the *Chrysophyte* were the most relevant taxa to increase in abundance throughout the photocatalytic treatment. The antioxidant activity from both *Chrysophyte* genera is unclear and any report that could explain this specific response against ROS could not be found. However, it is known that other *Chrysophyte* species from marine environment present a pronounced ability to produce lipopolysaccharide and carotenoids, such as fucoxanthin, which produces a high antioxidant response, considering both ROS quenching as well as photo-damage protection (Méresse et al., 2020; Sun et al., 2014). The increased abundance of this group in the treatment conditions may be linked to an intrinsic resistance or can reflect the impact on the microbial plankton community composition, including the decrease of the originally dominant cyanobacteria and zooplankton. Also, these organisms could have taken advantage of the altered abiotic environmental conditions that occurred as a result of the treatment, e.g., increased light availability due to a decrease in turbidity and increase in transparency. Although these organisms are mixotrophic, they present a pronounced heterotrophy activity with limited use of light as energy source (Graupner et al., 2018). For example, in North America lakes, *Chrysophyte* species are commonly found in oligo- and mesotrophic environments where their competitive ability in phosphorous limitation allows them to dominate the planktonic community over other algae (Nicholls and Wujek, 2003). Although we did not observe any change in nutrient content, this group could dominate the eukaryote community due to other factors besides microbial composition, such as DOC dynamics, their mixotrophic characteristics, as well as the increased light availability in the photocatalytic system.

Interestingly, *Ochromonas* have been identified as *Microcystis* grazers and a microcystin (cyanotoxin) degrader after an ultrasound-assisted process was used at lab scale to estimate its application for water cleaning and cyanobacteria controlling (Zhang et al., 2021, 2018). Alternatively, the treatment could stimulate an indirect control of cyanobacteria and a potential microcystin degradation by promoting an increase in Ochromonas abundance. This fact indicates the importance of investigating the ecological role of microbial communities resistant to alternative treatments and their capacity for degrading diverse toxic compounds that may be released after treatment.

3.3. Relationship between biotic and abiotic parameters

In this study, we tested for correlation between relevant abiotic parameters affected by the treatment and selected taxa, corresponding to the susceptible or resistant bacterial and eukaryotic taxa (high LDA scores according to the LEfSe analysis at T7) including the main cyanobacterial genera observed in 16S rRNA data. We used a canonical correspondence analysis (CCA) coupled to Spearman correlation ($p<0.05$) (Fig. 6 and Table S8).

For the bacterioplankton, the CCA ordination had the total variation of data explained by the two main axes (82 and 14%, respectively) with a significant p-value for their eigenvalues ($p=0.01$ and 0.02, respectively).

A strict relationship was observed between turbidity and all cyanobacterial genera sharing the same dimensional quadrant, which considered all sampling times for the control condition, including T0 (Fig. 6A), in which cyanobacteria maintained high relative abundance. This was confirmed by the Spearman analysis, showing a significant positive correlation between turbidity and cyanobacteria with high r-values for *Planktothrix* and *Microcystis* ($r=0.67$ for both) as well as *Raphidiopsis* and *Sphaerospermospsis* ($r=0.54$ for both) (Table S8). For transparency, *Microcystis* presented a significant negative correlation ($r=0.61$), as well as *Cyanobium* and *Nodosilinea* ($r= -0.60$ and -0.66, respectively). The resistant bacteria *Asinibacterium* and *Prosthecobacter* presented significant negative correlations with turbidity ($r= -0.74$ and -0.45, respectively) and a positive correlation with transparency ($r=0.57$ and 0.44, respectively).

The association between cyanobacterial dynamics and the improvement of turbidity and transparency was previously observed from the use of H_2O_2 in Gavião reservoir (Santos et al., 2021) where the chlorophyll content of these organisms decreased over time simultaneously with an increase in transparency.

Other abiotic parameters such as dissolved oxygen and pH also presented a positive correlation with susceptible cyanobacterial genera and negative correlations with resistant bacteria. For dissolved oxygen the correlation was significant for *Microcystis* ($r= 0.51$), *Planktothrix* ($r= 0.50$) and *Sphaerospermopsis* ($r= 0.53$) and for the resistant *Asinibacterium* ($r= -0.55$) and *Prosthecobacter* ($r= -0.46$). For pH, significant correlations were found for the cyanobacteria *Leptolyngbyaceae_uncl*: ($r= 0.68$), *Prochlorothrix* ($r= 0.50$) and *Raphidiopsis* ($r= 0.44$) and for the resistant taxa Flectobacillus ($r= 0.51$) (Fig. 6A and Table S7).

Organic carbon content (TOC and DOC) presented negative correlation with the cyanobacteria *Cyanobium* and *Microcystis* ($r=0.45$ and 0.53, respectively) and with the heterotrophic bacteria CL500_3 and

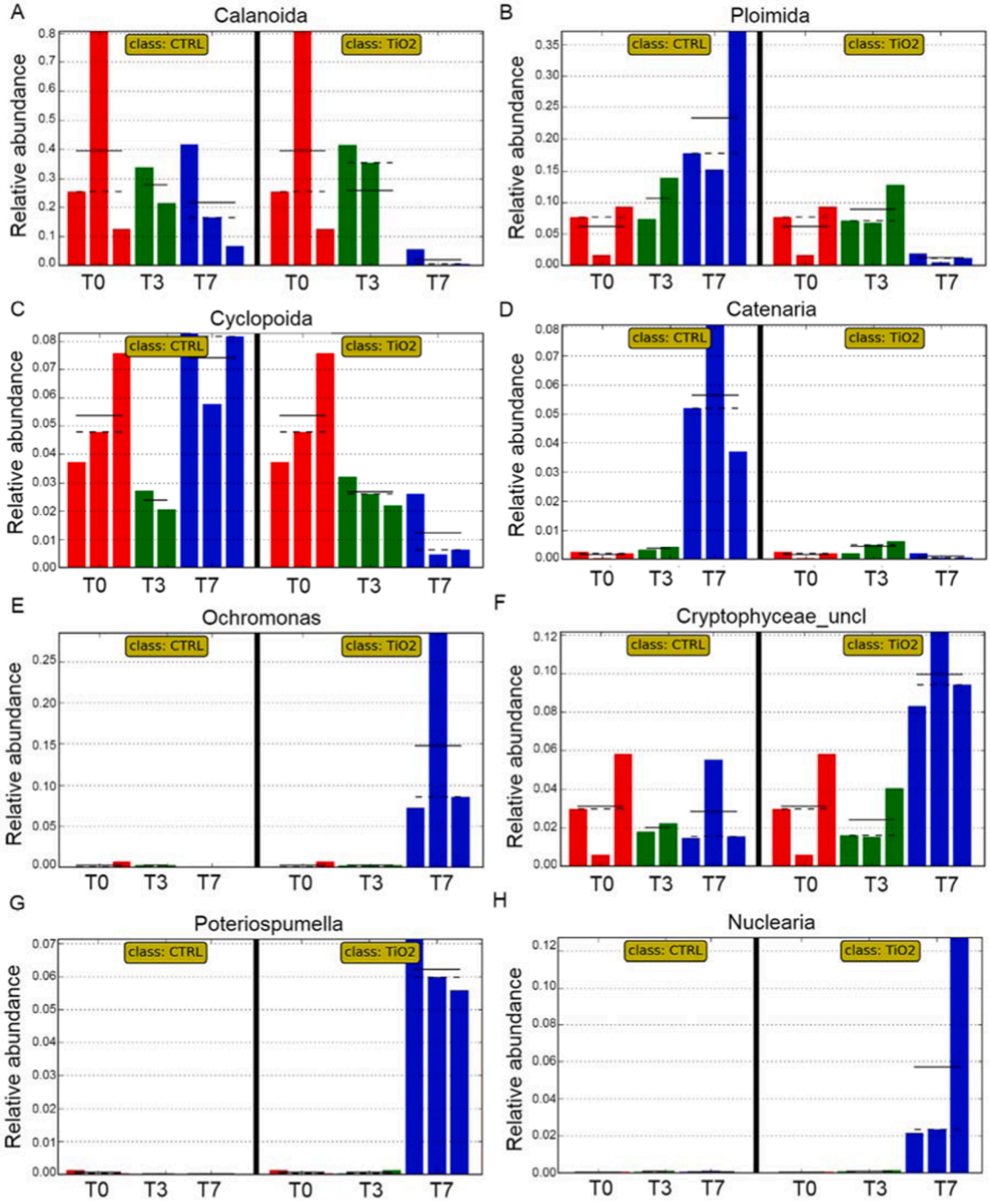

Fig. 5. Differential abundance of eukaryote taxa affected by TiO_2 compared to the control condition according to LEfSe analysis ($p < 0.05$), considering susceptible (A–D) and resistant organisms (E–H). The different colors express the sampling days T0 (red), T3 (green) and T7 (blue). Data are represented as means of triplicates except for T3, as those samples presented a very low number of sequences. Full black lines represent the average of three samples, the dashed black line represents the median.

LD29 (r=0.47 and 0.58, respectively), whereas *Prosthecobacter*, a resistant bacterium, showed positive correlation with TOC and DOC (r=0.61 and 0.49, respectively; Table S8). This relationship between TOC/DOC and bacteria, among cyanobacteria and heterotrophic ones, could be associated to the photodegradation and lysis of susceptible cyanobacteria while other bacteria could be involved in the biodegradation of intracellular products released to the water (Huang et al., 2017; Ye et al., 2015). Farkas et al. (2015) observed a strict relationship between the TiO_2 nanoparticles and organic carbon affecting the bacterial community, where lakes with higher concentrations of DOC and lower chemical element concentrations presented a significant reduction of bacterial abundance and activity. Although we identified a positive correlation between some resistant taxa (among bacteria and eukaryote) and DOC, we could not establish the influence of carbon on the treatment efficiency.

In the eukaryotic community, CCA showed a discrete ordination of taxa and abiotic parameters with fewer relationships when compared to the bacterioplankton (Fig. 6B). The two main axes explained the total variation of data, contributing with 69 and 21%, respectively, and significant p-values (p=0.002 and 0.1, respectively).

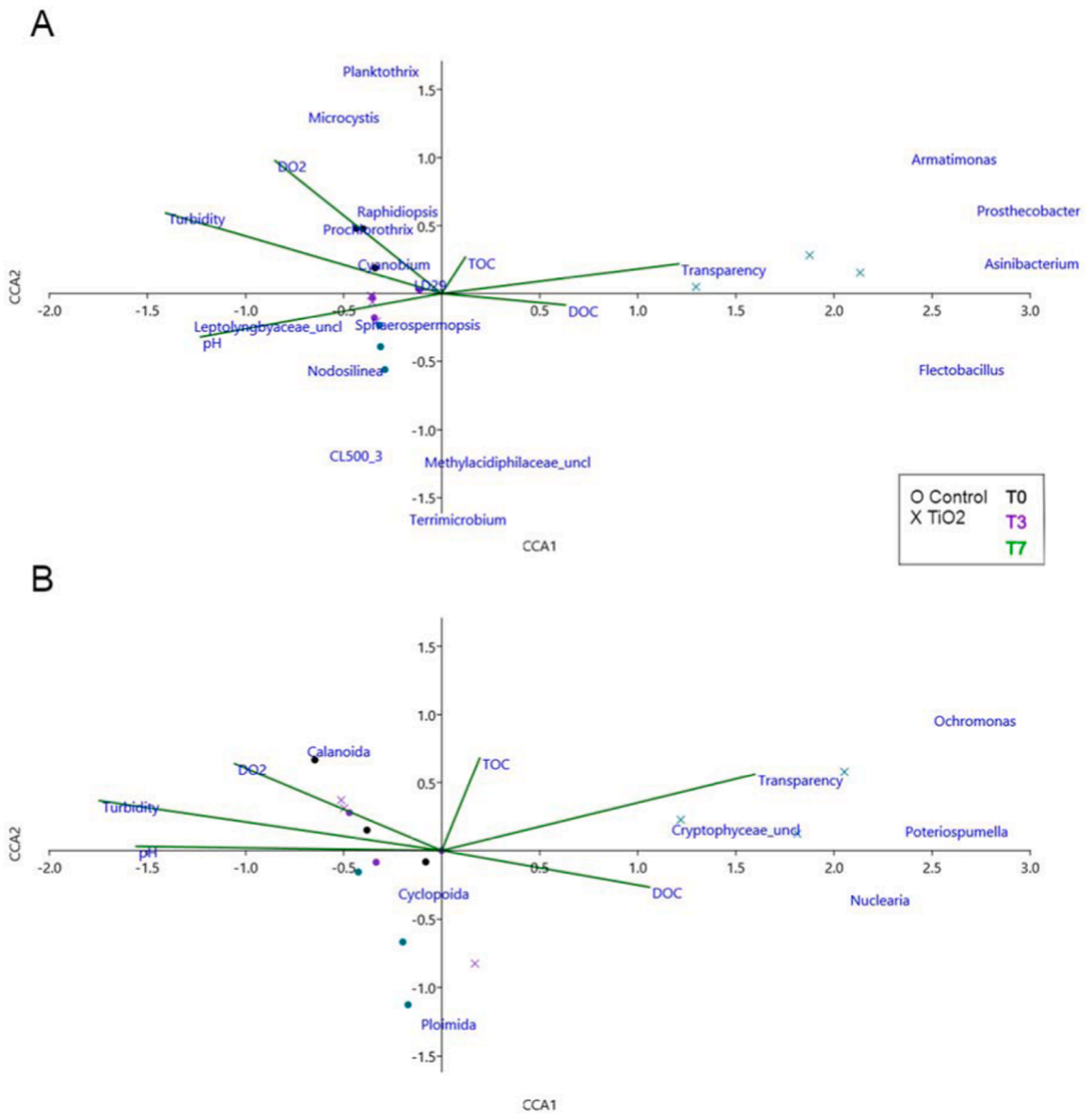

Fig. 6. Canonical correspondence analysis (CCA) considering the relevant physico-chemical parameters affected by the treatment over time and the main susceptible and resistant genera from the bacterial (A) and eukaryotic (B) plankton communities. Taxa used as input here were from sequencing data that contributed to the differentiation between control and treatment according to the highest LDA scores from LEfSe analysis ($p < 0.05$).

Cyclopoida was the only susceptible taxon located opposite transparency topresent a negative correlation with this parameter (r= -0.54). In contrast, the resistant *Ochromonas, Poteriospumella* and *Nuclearia* were located close to transparency, in the opposite quadrant (Fig. 6B). *Ochromonas* (r=0.58) and *Nuclearia* (r=0.55) were positively correlated with transparency, whereas *Poteriospumella* was negatively correlated with turbidity (r=-0.44). *Ochromonas* and *Nuclearia* also showed positive correlation with TOC and DOC (r=0.47 and 0.58, respectively, for *Ochromonas* and r=0.55 and 0.53, respectively, for *Nuclearia*) (Table S8).

3.4. *In situ application of TiO_2-based photocatalysis*

For over twenty five years, the potential of TiO_2 photocatalysis as a promising technology for the control of cyanobacteria and their toxins has been described in the literature (Lawton et al., 1999; Robertson et al., 1997, 1998a). Much of the work, however, has involved lab scale applications with only a small number of reports detailing pilot scale reactor studies (Menezes et al., 2021; Pestana et al., 2014). Consequently, much of the work reported has been at lower Technology Readiness Levels (TRLs) between 1 and 3. To move this technology further up the TRL scale, larger scale applications capable of treating cubic meter quantities of water, will need to be demonstrated. In this paper, for the first time, the technology has been demonstrated to be a feasible *in situ* treatment step capable of larger scale water treatment hence moving the photocatalytic process up the TRL scale from four to five. It is envisioned that, continuous or as-needed-treatment with the proposed system adjacent to the WTP abstraction point could ease the cyanobacterial burden on the treatment plant. The removal of cyanobacteria and the intrinsic improvement of water quality could significantly decrease the need for treatment chemicals which is economically and environmentally favorable. The exact number of treatment units required would be determined on a case-by-case basis dependent on local conditions and incoming raw water quality/cyanobacterial load. Considerations of the potential inherent cost of the deployment system can be found in the Supplementary information (S8). Previous work has

clearly demonstrated that the proposed technology can remove both cyanobacteria and dissolved cyanotoxins (Gunaratne et al., 2020; Pestana et al., 2020c). This markedly decreases the public health dangers posed by toxic cyanobacterial blooms and could potentially also mitigate the effects of cyanobacteriogenic taste and odor episodes, as the removal of taste and odor compounds by TiO_2 photocatalysis has described before (Pestana et al., 2014, 2020b).

Post-treatment testing has demonstrated that the coating on the beads is stable (Figs. S5 and S6). It was observed that iron and manganese were incorporated into the elemental composition of the TiO_2-coated beads, which is most likely from components of the treatment unit. The photocatalytic efficiency of the used beads was tested against methylene blue in the laboratory (Fig. S7) and a 20% drop in removal efficiency was observed, most likely due to the aforementioned contamination with Fe and Mn. For future iterations of this treatment system, materials will have to be carefully selected to avoid affecting the photocatalytic efficiency.

In the current study, we observed alterations in the phyto- and zooplankton communities as a result of the photocatalytic treatment. Whether any changes would affect the microbial community in a water body the size of a drinking water reservoir would have to be carefully examined in due course. It is worth bearing in mind, however, that any type of intervention (e.g., limiting nutrient input or application of broad-spectrum algaecides) will have a knock-on effect on the micro-biosphere of a water body and will have to be carefully evaluated to balance the desired effects. A potential additional area of concern is the effect of the treatment on disinfection by-product formation. The effect of the TiO_2-photocatalysis in this regard will have to be carefully monitored and coordinated with carefully dialed-in treatment conditions in the disinfection step. Furthermore, as the treatment solution presented here is designed to be operated continuously the danger of re-growth of undesirable species is low compared to periodic treatments such as the application of algaecides or H_2O_2.

In the future, it would be desirable to power the lighting array with renewable energy systems such as photovoltaic or wind power depending on the local climatic conditions. A promising approach would be the deployment of floating photovoltaic units that feed a battery system, allowing for 24 h operation of the photocatalytic units. An additional advantage of the application of floating photovoltaic units would be the shading of the underlying water, further limiting cyanobacterial growth. Although the environmental impact of the use of photovoltaic units would have to be assessed against the benefits of their employment (Farrell et al., 2020). The application of the treatment units is not limited to the reservoir alone. While it is envisaged that this will be the main deployment point, deployment in settling tanks or on top of filter units within the conventional water treatment unit processes could unlock further potential to polish water and decrease treatment costs by increasing filter-life and decreasing the demand for chemical disinfection.

4. Conclusion

To ultimately ease the burden on water treatment plants an innovative TiO_2-UV LED reactor system was tested at mesocosm scale. Within seven days cyanobacterial abundance was reduced by 85% and water quality parameters like transparency and turbidity improved markedly. The current study represents a move towards bridging the gap between decades of academic laboratory-based research towards real life deployment of the technology, pushing the TRL further up the scale.

The proposed photocatalytic system aims to be sustainable with readily available and recycled constituent parts. Off-the-shelve components were used to construct the reactor system complimented by a facile photocatalyst deposition method onto beads made from post-consumer glass. While the treatment units were powered by mains power in the current study, there is scope to utilize renewable energy systems to further enhance the sustainability aspect.

Due to the flexibility the system offers (reactor length could be increased or decreased as required) other applications can be envisaged including deployment on top of filters within conventional water treatment plants as well as a polishing technology of product water and within product water storage.

Areas for future research include full lake trials, long-term effect on the ecosystem, life cycle analysis and techno-economic assessment to further push the treatment system up the TRL scale.

To conclude, we have, for the first time, demonstrated practical application of TiO_2-based photocatalysis at mesocosm scale under environmental conditions, allowing future development of *in situ* treatment for the reduction of cyanobacteria and their toxins.

Declaration of Competing Interest

The authors declare that they have no known competing financial interests or personal relationships that could have influenced the work reported in this paper.

Data availability

Data will be made available on request.

Acknowledgments

The authors would like to acknowledge the Engineering and Physical Sciences Research Council (EPSRC) [EP/P029280/1], the Coordination for the Improvement of Higher Education Personnel - CAPES [PROEX 20/2016 and Print 88887.311806/2018-00], the Brazilian National Research Council – CNPq [403116/2016-3 and 304164/2017-8] and the Ceará Research Support Foundation - FUNCAP [PNE-0112-00042.01.00/16] for funding this research.

Supplementary materials

Supplementary material associated with this article can be found, in the online version, at doi:10.1016/j.watres.2022.119299.

References

Amaral-Zettler, L.A., McCliment, E.A., Ducklow, H.W., Huse, S.M., 2009. A method for studying protistan diversity using massively parallel sequencing of V9 hypervariable regions of small-subunit ribosomal RNA Genes. PLoS One 4. https://doi.org/10.1371/journal.pone.0006372.

Andrews, S., 2010. FastQC: A Quality COntrol Toll for High Throughput Sequence Data [WWW Document]. URL http://www.bioinformatics.babraham.ac.uk/projects/fastqc.

Asker, D., Awad, T.S., Beppu, T., Ueda, K., 2012. Isolation, characterization, and diversity of novel radiotolerant carotenoid-producing bacteria. Methods Mol. Biol. 892, 21–60. https://doi.org/10.1007/978-1-61779-879-5_3.

Båmstedt, U., Larsson, H., 2018. An indoor pelagic mesocosm facility to simulate multiple water-column characteristics. Int. Aquat. Res. 10, 13–29. https://doi.org/10.1007/s40071-017-0185-y.

Barros, M.U.G., Wilson, A.E., Leitão, J.I.R., Pereira, S.P., Buley, R.P., Fernandez-Figueroa, E.G., Capelo-Neto, J., 2019. Environmental factors associated with toxic cyanobacterial blooms across 20 drinking water reservoirs in a semi-arid region of Brazil. Harmful Algae 86, 128–137. https://doi.org/10.1016/j.hal.2019.05.006.

Bernroitner, M., Zamocky, M., Furtmüller, P.G., Peschek, G.A., Obinger, C., 2009. Occurrence, phylogeny, structure, and function of catalases and peroxidases in cyanobacteria. J. Exp. Bot. 60, 423–440. https://doi.org/10.1093/jxb/ern309.

Callahan, B., 2018. Silva taxonomic training data formatted for DADA2 (Silva version 132). 10.5281/ZENODO.1172783.

Callahan, B.J., McMurdie, P.J., Holmes, S.P., 2017. Exact sequence variants should replace operational taxonomic units in marker-gene data analysis. ISME J. 11, 2639–2643. https://doi.org/10.1038/ismej.2017.119.

Callahan, J.B., McMurdie, J.P., Rosen, J.M., Han, W.A., Johnson, A.A.J., Holmes, P.S., 2016. Dada2: High resolution sample inference from Illumina amplicon data. Nat. Methods 13, 1–16.

Camacho-Muñoz, D., Fervers, A.S., Pestana, C.J., Edwards, C., Lawton, L.A., 2020. Degradation of microcystin-LR and cylindrospermopsin by continuous flow UV-A photocatalysis over immobilised TiO_2. J. Environ. Manag. 276 https://doi.org/10.1016/j.jenvman.2020.111368.

Caporaso, J.G., Lauber, C.L., Walters, W.A., Berg-Lyons, D., Lozupone, C.A., Turnbaugh, P.J., Fierer, N., Knight, R., 2011. Global patterns of 16S rRNA diversity at a depth of millions of sequences per sample. Proc. Natl. Acad. Sci. USA 108, 4516–4522. https://doi.org/10.1073/PNAS.1000080107/-/DCSUPPLEMENTAL/PNAS.201000080SI.PDF.

Cavalier-Smith, T., 2018. Kingdom Chromista and its eight phyla: a new synthesis emphasising periplastid protein targeting, cytoskeletal and periplastid evolution, and ancient divergences. Protoplasma 255, 297–357. https://doi.org/10.1007/s00709-017-1147-3.

Chun, S.J., Cui, Y., Lee, C.S., Ra Cho, A., Baek, K., Choi, A., Ko, S.R., Lee, H.G., Hwang, S., Oh, H.M., Ahn, C.Y., 2019. Characterization of distinct cyanohabs-related modules in microbial recurrent association network. Front. Microbiol. 10 https://doi.org/10.3389/fmicb.2019.01637.

Clemente, A., Wilson, A., Oliveira, S., Menezes, I., Gois, A., Capelo-Neto, J., 2020. The role of hydraulic conditions of coagulation and flocculation on the damage of cyanobacteria. Sci. Total Environ. 740, 139737 https://doi.org/10.1016/j.scitotenv.2020.139737.

Dokulil, M.T., Teubner, K., 2000. Cyanobacterial dominance in lakes. Hydrobiologia 438, 1–12.

Drábková, M., Admiraal, W., Maršálek, B., 2007. Combined exposure to hydrogen peroxide and light - selective effects on cyanobacteria, green algae, and diatoms. Environ. Sci. Technol. 41, 309–314. https://doi.org/10.1021/es060746i.

Fan, F., Shi, X., Zhang, M., Liu, C., Chen, K., 2019. Comparison of algal harvest and hydrogen peroxide treatment in mitigating cyanobacterial blooms via an *in situ* mesocosm experiment. Sci. Total Environ. 694 https://doi.org/10.1016/j.scitotenv.2019.133721.

Fan, J., Ho, L., Hobson, P., Brookes, J., 2013. Evaluating the effectiveness of copper sulphate, chlorine, potassium permanganate, hydrogen peroxide and ozone on cyanobacterial cell integrity. Water Res. 47, 5153–5164. https://doi.org/10.1016/j.watres.2013.05.057.

Fan, J., Hobson, P., Ho, L., Daly, R., Brookes, J., 2014. The effects of various control and water treatment processes on the membrane integrity and toxin fate of cyanobacteria. J. Hazard. Mater. 264, 313–322. https://doi.org/10.1016/j.jhazmat.2013.10.059.

Farkas, J., Peter, H., Ciesielski, T.M., Thomas, K.V., Sommaruga, R., Salvenmoser, W., Weyhenmeyer, G.A., Tranvik, L.J., Jenssen, B.M., 2015. Impact of TiO_2 nanoparticles on freshwater bacteria from three Swedish lakes. Sci. Total Environ. 535, 85–93. https://doi.org/10.1016/j.scitotenv.2015.03.043.

Farrell, C.C., Osman, A.I., Doherty, R., Saad, M., Zhang, X., Murphy, A., Harrison, J., Vennard, A.S.M., Kumaravel, V., Al-Muhtaseb, A.H., Rooney, D.W., 2020. Technical challenges and opportunities in realising a circular economy for waste photovoltaic modules. Renew. Sustain. Energy Rev. 128, 109911 https://doi.org/10.1016/J.RSER.2020.109911.

Graupner, N., Jensen, M., Bock, C., Marks, S., Rahmann, S., Beisser, D., Boenigk, J., 2018. Evolution of heterotrophy in chrysophytes as reflected by comparative transcriptomics. FEMS Microbiol. Ecol. 94 https://doi.org/10.1093/femsec/fiy039.

Grossman, A.R., Bhaya, D., Apt, K.E., Kehoe, D.M., 1995. Light-harvesting complexes in oxygenic photosynthesis: diversity, control, and evolution. Annu. Rev. Genet. https://doi.org/10.1146/annurev.ge.29.120195.001311.

Guedes, I.A., Rachid, C.T.C.C., Rangel, L.M., Silva, L.H.S., Bisch, P.M., Azevedo, S.M.F.O., Pacheco, A.B.F., 2018. Close link between harmful cyanobacterial dominance and associated bacterioplankton in a tropical eutrophic reservoir. Front. Microbiol. 9 https://doi.org/10.3389/fmicb.2018.00424.

Guillou, L., Bachar, D., Audic, S., Bass, D., Berney, C., Bittner, L., Boutte, C., Burgaud, G., De Vargas, C., Decelle, J., Del Campo, J., Dolan, J.R., Dunthorn, M., Edvardsen, B., Holzmann, M., Kooistra, W.H.C.F., Lara, E., Le Bescot, N., Logares, R., Mahé, F., Massana, R., Montresor, M., Morard, R., Not, F., Pawlowski, J., Probert, I., Sauvadet, A.L., Siano, R., Stoeck, T., Vaulot, D., Zimmermann, P., Christen, R., 2013. The Protist Ribosomal Reference database (PR2): A catalog of unicellular eukaryote Small Sub-Unit rRNA sequences with curated taxonomy. Nucleic Acids Res. 41 https://doi.org/10.1093/nar/gks1160.

Gunaratne, H.Q.N., Pestana, C.J., Skillen, N., Hui, J., Saravanan, S., Edwards, C., Irvine, J.T.S., Robertson, P.K.J., Lawton, L.A., 2020. All in one' photo-reactor pod containing TiO_2 coated glass beads and LEDs for continuous photocatalytic destruction of cyanotoxins in water. Environ. Sci. Water Res. Technol. 6, 945–950. https://doi.org/10.1039/c9ew00711c.

Hammer, Ø., Harper, D.A.T., Ryan, P.D., 2001. Past: Paleontological statistics software package for education and data analysis. Palaeontol. Electron. 4, 9–17.

Hitzfeld, B.C., Höger, S.J., Dietrich, D.R., 2000. Cyanobacterial toxins: Removal during drinking water treatment, and human risk assessment. Environ. Health Perspect. https://doi.org/10.1289/ehp.00108s1113.

Hoffmann, M.R., Martin, S.T., Choi, W., Bahnemann1', D.W., Keck, W.M., 1995. Environmental applications of semiconductor photocatalysis. Chem. Rev. 95, 69–96.

Huang, C., Yunmei, L., Liu, G., Guo, Y., Yang, H., Zhu, A.X., Song, T., Huang, T., Zhang, M., Shi, K., 2017. Tracing high time-resolution fluctuations in dissolved organic carbon using satellite and buoy observations: case study in Lake Taihu, China. Int. J. Appl. Earth Obs. Geoinf. 62, 174–182. https://doi.org/10.1016/J.JAG.2017.06.009.

Huang, W.J., Lin, T.P., Chen, J.S., Shih, F.H., 2011. Photocatalytic inactivation of cyanobacteria with ZnO/γ-Al2O3composite under solar light. J. Environ. Biol. 32, 301–307.

INMET - National Institute of Meteorology (Brazil), 2019. Weather data, [WWW Document]. URL http://www.inmet.gov.br/portal/index.php?r=bdmep/bdmep.

Lawton, L.A., Robertson, P.K.J., Cornish, B.J.P.A., Jaspars, M., 1999. Detoxification of microcystins (cyanobacterial hepatotoxins) using TiO_2 photocatalytic oxidation. Environ. Sci. Technol. 33, 771–775. https://doi.org/10.1021/es9806682.

Lawton, L.A., Robertson, P.K.J., Cornish, B.J.P.A., Marr, I.L., Jaspars, M., 2003. Processes influencing surface interaction and photocatalytic destruction of microcystins on titanium dioxide photocatalysts. J. Catal. 213, 109–113. https://doi.org/10.1016/S0021-9517(02)00049-0.

Li, Y., Lv, K., Ho, W., Dong, F., Wu, X., Xia, Y., 2017. Hybridization of rutile TiO_2 ($rTiO_2$) with g-C_3N_4 quantum dots (CN QDs): An efficient visible-light-driven Z-scheme hybridized photocatalyst. Appl. Catal. B Environ. 202, 611–619. https://doi.org/10.1016/j.apcatb.2016.09.055.

Litchman, E., Edwards, K.F., Klausmeier, C.A., 2015. Microbial resource utilization traits and trade-offs: Implications for community structure, functioning, and biogeochemical impacts at present and in the future. Front. Microbiol. 6 https://doi.org/10.3389/fmicb.2015.00254.

Liu, I., Lawton, L.A., Robertson, P.K.J., 2003. Mechanistic studies of the photocatalytic oxidation of microcystin-LR: an investigation of byproducts of the decomposition process. Environ. Sci. Technol. 37, 3214–3219. https://doi.org/10.1021/es0201855.

Liu, L., Chen, H., Liu, M., Yang, J.R., Xiao, P., Wilkinson, D.M., Yang, J., 2019. Response of the eukaryotic plankton community to the cyanobacterial biomass cycle over 6 years in two subtropical reservoirs. ISME J. 13, 2196–2208. https://doi.org/10.1038/s41396-019-0417-9.

Loeb, S.K., Alvarez, P.J.J., Brame, J.A., Cates, E.L., Choi, W., Crittenden, J., Dionysiou, D. D., Li, Q., Li-Puma, G., Quan, X., Sedlak, D.L., David Waite, T., Westerhoff, P., Kim, J. H., Byers, B., 2019. The technology horizon for photocatalytic water treatment: sunrise or sunset? Environ. Sci. Technol. 53, 45. https://doi.org/10.1021/acs.est.8b05041.

Marques, É.T., Gunkel, G., Sobral, M.C., 2019. Management of tropical river basins and reservoirs under water stress: experiences from northeast Brazil. Environ. MDPI 6. https://doi.org/10.3390/environments6060062.

Martin, M., 2011. Cutadapt removes adapter sequences from high-throughput sequencing reads. EMBnet.Journal. https://doi.org/10.14806/ej.17.1.200.

Martínez-Laborda, A., Balsalobre, J.M., Fontes, M., Murillo, F.J., 1990. Accumulation of carotenoids in structural and regulatory mutants of the Bacterium *Myxococcus xanthus*. MGG Mol. Gen. Genet. 223, 205–210. https://doi.org/10.1007/BF00265055.

Menezes, I., Capelo-Neto, J., Pestana, C.J., Clemente, A., Hui, J., Irvine, J.T.S., Nimal Gunaratne, H.Q., Robertson, P.K.J., Edwards, C., Gillanders, R.N., Turnbull, G.A., Lawton, L.A., 2021. Comparison of UV-A photolytic and UV/TiO_2 photocatalytic effects on *Microcystis aeruginosa* PCC7813 and four microcystin analogues: a pilot scale study. J. Environ. Manag. 298, 113519 https://doi.org/10.1016/j.jenvman.2021.113519.

Méresse, S., Fodil, M., Fleury, F., Chénais, B., 2020. Fucoxanthin, a marine-derived carotenoid from brown seaweeds and microalgae: a promising bioactive compound for cancer therapy. Int. J. Mol. Sci. https://doi.org/10.3390/ijms21239273.

Nicholls, K.H., Wujek, D.E., 2003. Chrysophycean algae. In: Wehr, J., Sheath, R., Kociolek, J.P. (Eds.), Freshwater Algae of North America: Ecology and Classification. Elsevier Inc. Academic Press, San Diego, CA, USA, pp. 471–509. https://doi.org/10.1016/B978-012741550-5/50013-1.

Paerl, H.W., Huisman, J., 2008. Climate: blooms like it hot. Science 320, 57–58. https://doi.org/10.1126/science.1155398 (80-.).

Passardi, F., Zamocky, M., Favet, J., Jakopitsch, C., Penel, C., Obinger, C., Dunand, C., 2007. Phylogenetic distribution of catalase-peroxidases: are there patches of order in chaos? Gene 397, 101–113. https://doi.org/10.1016/j.gene.2007.04.016.

Pestana, C.J., Capelo-Neto, J., Lawton, L., Oliveira, S., Carloto, I., Linhares, H.P., 2019. The effect of water treatment unit processes on cyanobacterial trichome integrity. Sci. Total Environ. 659, 1403–1414. https://doi.org/10.1016/j.scitotenv.2018.12.337.

Pestana, C.J., Hobson, P., Robertson, P.K.J., Lawton, L.A., Newcombe, G., 2020a. Removal of microcystins from a waste stabilisation lagoon: Evaluation of a packed-bed continuous flow TiO_2 reactor. Chemosphere 245, 125575. https://doi.org/10.1016/j.chemosphere.2019.125575.

Pestana, C.J., Lawton, L.A., Kaloudis, T., 2020b. Removal and/or Destruction of taste and odour compound by conventional and advanced oxidation processes. In: Hiskia, A. E., Triantis, T.M., Antoniou, M.G., Kaloudis, T., Dionysiou, D.D. (Eds.), Water Treatment for Purification from Cyanobacteria and Cyanotoxins. John Wiley & Sons Ltd, Hoboken, NJ, pp. 207–230.

Pestana, C.J., Portela Noronha, J., Hui, J., Edwards, C., Gunaratne, H.Q.N., Irvine, J.T.S., Robertson, P.K.J., Capelo-Neto, J., Lawton, L.A., 2020c. Photocatalytic removal of the cyanobacterium *Microcystis aeruginosa* PCC7813 and four microcystins by TiO_2 coated porous glass beads with UV-LED irradiation. Sci. Total Environ. 745, 141154 https://doi.org/10.1016/j.scitotenv.2020.141154.

Pestana, C.J., Robertson, P.K.J., Edwards, C., Wilhelm, W., McKenzie, C., Lawton, L.A., 2014. A continuous flow packed bed photocatalytic reactor for the destruction of 2-methylisoborneol and geosmin utilising pelletised TiO_2. Chem. Eng. J. 235, 293–298. https://doi.org/10.1016/j.cej.2013.09.041.

R Core Team, 2020. R: A Language and Environment for Statistical Computing [WWW Document]. R Found. Stat. Comput., Vienna, Austria. URL. https://www.r-project.org/.

Robertson, P.K.J., Lawton, L.A., Cornish, B.J.P.A., Jaspars, M., 1998a. Processes influencing the destruction of microcystin-LR by TiO_2 photocatalysis. J. Photochem. Photobiol. A Chem. 116, 215–219. https://doi.org/10.1016/S1010-6030(98)00312-8.

Robertson, P.K.J., Lawton, L.A., Cornish, B.J.P.A., 1998b. The involvement of phycocyanin pigment in the photodecomposition of the cyanobacterial toxin, microcystin-LR. J. Porphyrins Phthalocyanines 3, 544–551, 10.1002/(SICI)1099-1409(199908/10)3:6/7<544::AID-JPP173>3.0.CO;2-7.

Robertson, P.K.J., Lawton, L.A., Münch, B., Rouzade, J., 1997. Destruction of cyanobacterial toxins by semiconductor photocatalysis. Chem. Commun. 393–394. https://doi.org/10.1039/a607965b.

Rognes, T., Flouri, T., Nichols, B., Quince, C., Mahé, F., 2016. VSEARCH: a versatile open source tool for metagenomics. PeerJ 2016. https://doi.org/10.7717/peerj.2584.

Santos, A.A., Guedes, D.O., Barros, M.U.G., Oliveira, S., Pacheco, A.B.F., Azevedo, S.M.F. O., Magalhães, V.F., Pestana, C.J., Edwards, C., Lawton, L.A., Capelo-Neto, J., 2021. Effect of hydrogen peroxide on natural phytoplankton and bacterioplankton in a drinking water reservoir: Mesocosm-scale study. Water Res. 197, 117069 https://doi.org/10.1016/j.watres.2021.117069.

Simpson, A.G.B., Eglit, Y., 2016. Protist diversification. In: Kliman, R.M. (Ed.), Encyclopedia of Evolutionary Biology Volume 3. Elsevier, Amsterdam, pp. 344–360.

Slade, D., Radman, M., 2011. Oxidative stress resistance in *Deinococcus radiodurans*. Microbiol. Mol. Biol. Rev. 75, 133–191. https://doi.org/10.1128/mmbr.00015-10.

Stafsnes, M.H., Josefsen, K.D., Kildahl-Andersen, G., Valla, S., Ellingsen, T.E., Bruheim, P., 2010. Isolation and characterization of marine pigmented bacteria from Norwegian coastal waters and screening for carotenoids with UVA-blue light absorbing properties. J. Microbiol. 48, 16–23. https://doi.org/10.1007/s12275-009-0118-6.

Sun, L., Wang, L., Li, J., Liu, H., 2014. Characterization and antioxidant activities of degraded polysaccharides from two marine Chrysophyta. Food Chem. 160, 1–7. https://doi.org/10.1016/j.foodchem.2014.03.067.

Takebe, F., Hara, I., Matsuyama, H., Yumoto, I., 2007. Effects of H_2O_2 under low- and high-aeration-level conditions on growth and catalase activity in *Exiguobacterium oxidotolerans* T-2-2T. J. Biosci. Bioeng. 104, 464–469. https://doi.org/10.1263/jbb.104.464.

Tõnno, I., Agasild, H., Kõiv, T., Freiberg, R., Nõges, P., Nõges, T., 2016. Algal diet of small-bodied crustacean zooplankton in a cyanobacteria-dominated eutrophic lake. PLoS One 11, e0154526. https://doi.org/10.1371/journal.pone.0154526.

Tytler, E.M., Wong, T., Codd, G.A., 1984. Photoinactivation *in vivo* of superoxide dismutase and catalase in the cyanobacterium *Microcystis aeruginosa*. FEMS Microbiol. Lett. 23, 239–242. https://doi.org/10.1111/j.1574-6968.1984.tb01070.x.

Vaissie, P., Monge, A., Hudsson, F., 2020. Fac toshiny: Perform Factorial Analysis from "FactoMineR" with a Shiny Application. R-package version 2.2.

Winnepenninckx, B., Backeljau, T., De Wachter, R., 1993. Extraction of high molecular weight DNA from molluscs. Trends Genet. 9, 407. https://doi.org/10.1016/0168-9525(93)90102-n.

Yang, Z., Buley, R.P., Fernandez-Figueroa, E.G., Barros, M.U.G., Rajendran, S., Wilson, A. E., 2018. Hydrogen peroxide treatment promotes chlorophytes over toxic cyanobacteria in a hyper-eutrophic aquaculture pond. Environ. Pollut. 240, 590–598. https://doi.org/10.1016/j.envpol.2018.05.012.

Ye, L., Wu, X., Liu, B., Yan, D., Kong, F., 2015. Dynamics and sources of dissolved organic carbon during phytoplankton bloom in hypereutrophic Lake Taihu (China). Limnologica 54, 5–13. https://doi.org/10.1016/J.LIMNO.2015.05.003.

Yilmaz, P., Parfrey, L.W., Yarza, P., Gerken, J., Pruesse, E., Quast, C., Schweer, T., Peplies, J., Ludwig, W., Glöckner, F.O., 2014. The SILVA and "all-species Living Tree Project (LTP)" taxonomic frameworks. Nucleic Acids Res. 42 https://doi.org/10.1093/nar/gkt1209.

Zamyadi, A., Macleod, S.L., Fan, Y., Mcquaid, N., Dorner, S., Sauvé, S., Prévost, M., 2012. Toxic cyanobacterial breakthrough and accumulation in a drinking water plant: a monitoring and treatment challenge. Water Res. 46, 1511–1523. https://doi.org/10.1016/j.watres.2011.11.012.

Zhang, L., Lyu, K., Wang, N., Gu, L., Sun, Y., Zhu, X., Wang, J., Huang, Y., Yang, Z., 2018. Transcriptomic analysis reveals the pathways associated with resisting and degrading microcystin in ochromonas. Environ. Sci. Technol. 52, 11102–11113. https://doi.org/10.1021/acs.est.8b03106.

Zhang, L., Yang, J., Liu, L., Wang, N., Sun, Y., Huang, Y., Yang, Z., 2021. Simultaneous removal of colonial *Microcystis* and microcystins by protozoa grazing coupled with ultrasound treatment. J. Hazard. Mater. 420 https://doi.org/10.1016/j.jhazmat.2021.126616.

Zheng, Q., Wang, Y., Lu, J., Lin, W., Chen, F., Jiao, N., 2020. Metagenomic and metaproteomic insights into photoautotrophic and heterotrophic interactions in a *Synechococcus* culture. mBio 11. https://doi.org/10.1128/mBio.03261-19.

Supplementary Information for:

Selective suppression of cyanobacteria using TiO_2-based photocatalysis *in situ*: short term evaluation in a drinking water reservoir

Carlos J. Pestana[a*†], Allan Amorim Santos[b*], Samylla Oliveira[c], Ricardo Rogers[b], Jianing Hui[d], Nathan C. Skillen[e], Christine Edwards[a], José Capelo-Neto[c], Sandra M.F.O. Azevedo[b], Peter K.J. Robertson[e], John T.S. Irvine[d], Linda A. Lawton[a]

* These two authors have contributed equally to the manuscript

† corresponding author: c.pestana@rgu.ac.uk

[a] School of Pharmacy and Life Sciences, Robert Gordon University, Aberdeen, UK

[b] Institute of Biophysics Carlos Chagas Filho, Federal University of Rio de Janeiro, Rio de Janeiro, Brazil

[c] Department of Hydraulic and Environmental Engineering, Federal University of Ceará, Fortaleza, Brazil

[d] School of Chemistry, University of St. Andrews, St. Andrews, UK

[e] School of Chemistry and Chemical Engineering, Queen's University Belfast, Belfast, UK

S1 Meteorological Data

Table S1: Meteorological condition observed between October and November 2019 at Fortaleza city according to the National Institute of Meteorology – INMET. The data are expressed as averages from daily measurements.

Avg. Temp. (ºC)	Humidity (%)	Atmospheric pressure (hPa)	Wind velocity (m/s)	Solar irradiance (h)	Max. Temp. (ºC)	Min. Temp. (ºC)	Precipitation (mm)
27.7 ± 1.2	74 ± 8.7	1009.6 ± 1.2	3.01 ± 1.0	10.2 ± 0.7	32.2 ± 0.5	25.0 ± 0.6	0.05 ± 0.2

S2 Materials and Methods

S2.1 Physicochemical analyses

Table S2: Physical and chemical parameters measured *in situ* or in the laboratory (all methods apart from transparency determination according to APHA, 2012).

Parameter (unit)	Equipment/Method	Where
Transparency (cm)	Secchi disk	*in situ*
Temperature (°C) and pH	YSI probe model 55 and 60 (Yellow Springs Instruments, EUA) / APHA 4500 H-B	*in situ*
Dissolved oxygen (mg/L)	YSI probe model 55 (Yellow Springs Instruments, EUA) / APHA 4500 O-G	*in situ*
Conductivity (µS/cm)	Conductivity meter 105A+ (Orion Research, EUA) / APHA2510-A	*in situ*
Turbidity (NTU)	Hach model 2100P (EUA) / APHA2130-B	Laboratory
True color (uC)	Genesys spectrophotometer 10S UV-Vis – (Thermo Scientific, EUA) / APHA2120-C	Laboratory
Total organic carbon (TOC) and dissolved carbon (DOC) (mg L^{-1})	Sievers InnovOx Laboratory TOC Analyzer (General Electrics, USA) / APHA5310	Laboratory

Nitrite, nitrate, orthophosphate, sulfate, fluoride, and chloride (mg L^{-1}).	Samples were filtered through a glass fiber 0.45-µm membrane before analyses by Ion Chromatograph using Dionex ICS-1100 (Thermo Scientific, EUA) / APHA4110-C	Laboratory

S2.2 Statistical analysis

S2.2.1 Abiotic factors

Principal component analysis (PCA) was performed as a nonlinear multivariate statistical technique, used to determine the relationships between the physical and chemical environmental parameters analyzed from the control and treatment samples over time. PCA was also used to gather the data in groups according to their variances in the different dimensional axes (Savegnago et al., 2011). A selection of the parameters for PCA ordination was conducted following their importance related to the effect of the treatment as well as the size of the vector (considering cos^2 value) and the contribution with at least more than 70% of dimensionality variance from the principal components. Subsequently, clustering was carried out using the Canberra distance (Riba et al., 2020) and Ward's method.

For each physical and chemical parameter considered relevant from PCA and non-normal distribution (following Shapiro-Wilk $p<0.05$), a Wilcoxon-Mann-Whitney test was performed to show significant differences ($p<0.05$) between the two groups and identify, one by one, the parameters that could show the efficiency of the photocatalytic treatment with TiO_2. Statistical analyzes were performed using R software version 3.4.1, using the Factoshiny package (Vaissie et al., 2020).

S2.2.2 Biotic factors (bacterial and eukaryotic plankton communities)

Alpha-diversity estimators were calculated and tested for normality considering the Shapiro-Wilk test, skewness, and kurtosis, to evaluate significant differences between treatment and control at each sampling time. As Shannon diversity and estimated richness (observed species) from 16S rRNA data were parametric, a two-way analysis of variance test was used for multiple comparisons of means at a 95% confidence interval considering time and condition (treatment and control) as factors, whereas for 18S rRNA data, we used the Kruskal-Wallis non-parametric test.

From the 18S rRNA data, we used the taxonomic groups identified and gathered the main taxa (>3% relative abundance in at least one sample) in relevant freshwater plankton groups, following the classification described in previous studies (Cavalier-Smith, 2018; Simpson and Eglit, 2016) (Table S2).

The beta-diversity ordination was evaluated by nMDS (non-metric dimensional scaling) considering ASVs abundance in a tridimensional space using the Bray-Curtis distance as dissimilarity matrix. Then, it was complemented by permutational multivariate analysis of variance (two-way PERMANOVA, $p<0.05$) using two factors as experimental condition (control or TiO_2) and time (0, 3 and 7). In the null-hypothesis, TiO_2 did not affect the bacterial and eukaryotic plankton communities; alternatively, we assumed that the treatment modified the structure of both communities.

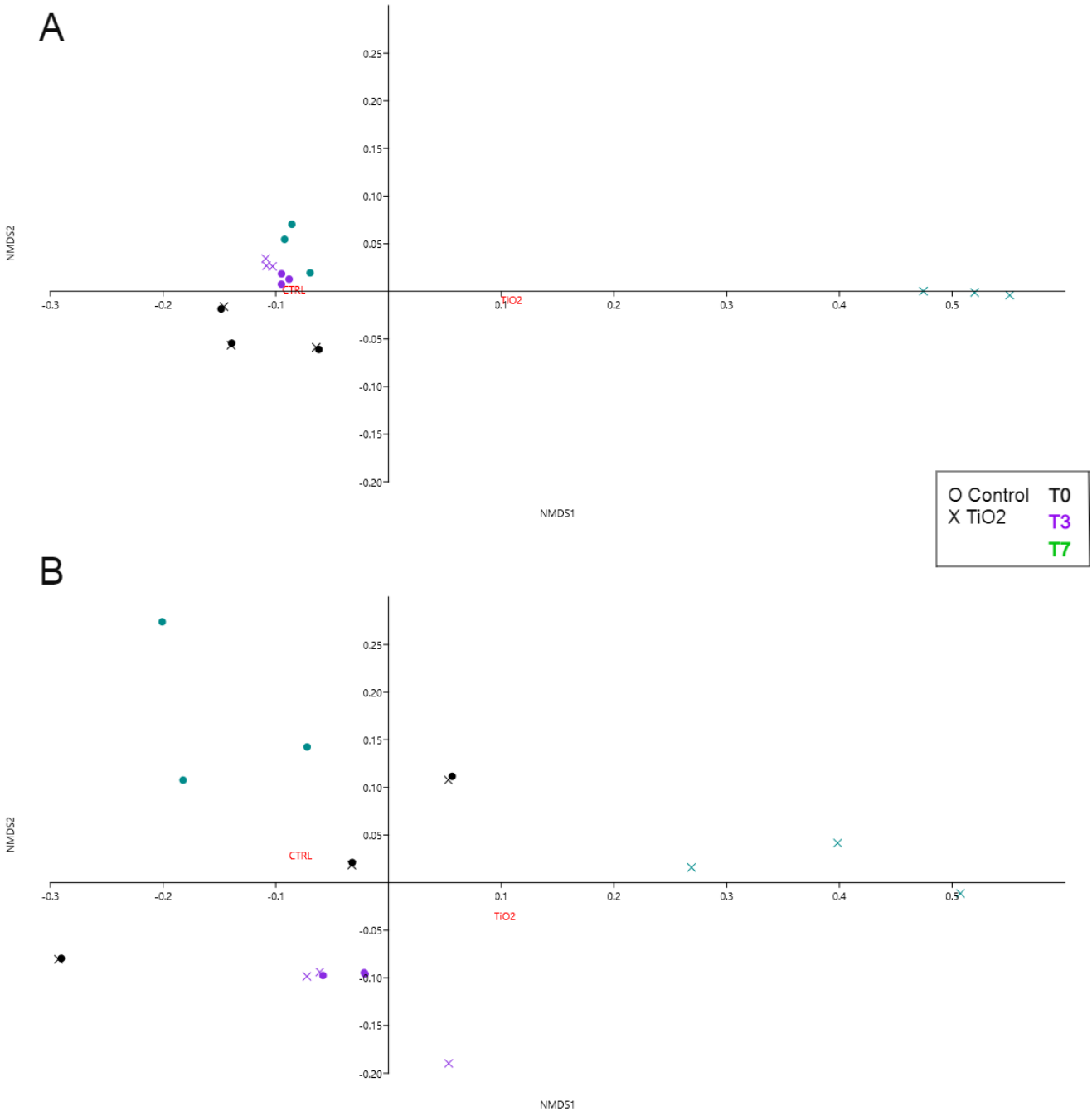

Figure S1: Beta diversity considering samples ordination according to the Bacteria (A) and Eukarya (B) composition by non-metric multidimensional scaling (nMDS) using Bray-Curtis distance. Samples correspond to control (circle) or TiO_2/UV treatment (X) collected over the time 0, 3 and 7 days (n=3).

Table S3: Internal assignment of most representative 18S taxa considering relevant groups of freshwater biotic system following taxonomic classification of Cavalier-Smith (2018) and Simpson and Eglit (2016).

Defined Groups	Representative Taxa	Kingdom	Phylum	Observed Genus
Chlorophyte	*Chlorophyta*	Plantae	*Chlorophyta*	Unclassified
Diatom	*Bacillariophyceae*	Chromista	*Bacillariophyta*	Nitzschia / Navicula / Unclassified
	Fragilariales		*Bacillariophyta*	Ulnaria / Unclassified
	Mediophyceae		*Bacillariophyta*	Cyclotella / Unclassified
Chrysophyte	*Chrysophyceae*		*Ochrophyta*	Unclassified
	Chromulinales		*Ochrophyta*	Poteriospumella / Poterioochromonas / Oikomonas / Unclassified
	Ochromonadales		*Ochrophyta*	Paraphysomonas / Ochromonas / Unclassified
Cryptophyte	*Cryptophyceae*		*Cryptophyta*	Unclassified
Alveolata	*Dinoflagellata*		*Miozoa*	Unclassified
	Perkinsidae		*Miozoa*	Unclassified
Alveolata	*Colpodellida*		*Miozoa*	Colpodella
	Choreotrichia		*Ciliophora*	Tintinnidium / Unclassified
	Hypotrichia		*Ciliophora*	Halteria / Oxytricha / Stylonychia / Pseudourostyla / Unclassified
Discicristata/ Euglenid	*Neobodonida*	Protozoa	*Euglenozoa*	Rhynchobodo / Neobodo / Rhynchomonas / Unclassified
	Prokinetoplastina		*Euglenozoa*	Ichthyobodo
	Discicristata		*Uncertain*	Unclassified
Nucleariids	*Nucleariidae*		*Choanozoa*	Unclassified
Zooplakton	*Gastrotricha*	Animalia	*Gastrotricha*	Nuclearia / Unclassified
	Copepoda		*Arthropoda*	Calanoida / Cyclopoida / Unclassified
	Podocopa		*Arthropoda*	Unclassified
	Monogononta		*Rotifera*	Ploimida / Floscularia / Unclassified
Fungi	*Blastocladiales*	Fungi	*Blastocladiomycota*	Catenaria
Eukaryotic picoplankton	*Eukaryotic_ picoplankton_ environmental_ sample*	Uncertain	*Uncertain*	Unclassified
Unclassified	*MAST_12C*		*Uncertain*	Unclassified
	Incertae_division		*Uncertain*	Unclassified
Eukarya_uncl	*Eukarya_uncl*		*Uncertain*	Unclassified
Stramenopiles_ uncl	*Stramenopiles_ uncl*	Chromista	*Stramenopiles*	Unclassified

We also performed a linear discriminant analysis (LDA) and effect Size (LEfSe) (Segata et al., 2011) following the Hutlab Galaxy web framework (http://huttenhower.sph.harvard.edu/galaxy/) using 3.5 as LDA threshold (log 10 transformed) to select microbial taxa with a significant contribution ($p<0.05$) to the differentiation between treatment and control. For that, we applied a two-tailed non-parametric Kruskal-Wallis test and unpaired Wilcoxon test to reveal significant differences in most abundant ASVs.

S2.3 Correlation between biotic and abiotic factors

To test the correlation between abiotic and biotic (ASVs) factors and differences in the community structure over time, the samples were ordained by Canonical Correspondence Analysis (CCA) using the Hellinger-transformed abundance matrix and Spearman analysis ($p<0.05$ and a threshold for r value $=\pm0.4$). The analyses were performed, and charts plotted in R v3.5.3 environment (R Core Team, 2016) and Past3 software (Hammer et al., 2001).

S3 Effect of TiO_2-photocatalysis on bacterioplankton

Table S4: Relative abundance of bacterioplankton at phylum level, considering mean and standard deviation (n=3) expressed as percentage (%) of total bacterioplankton. * Taxa classified as 'Others' in the abundance chart.

Phylum	T0	Day 3		Day 7	
		Control	TiO_2	Control	TiO_2
*Acidobacteria**	0.1±0.02	0.1±0.003	0.2±0.05	0.05±0.02	0.6±0.2
Actinobacteria	0.9±0.32	3.8±0.48	4.4±0.22	5.4±0.45	4±0.75
*Armatimonadetes**	0.4±0.33	0.5±0.7	0.2±0.04	0.2±0.12	6.8±1.56
Bacteroidetes	13.6±3.2	14.9±1.6	14±1.23	10.7±2.9	35±4.94
*Chlamydiae**	0.01±0.003	0.08±0.01	0.07±0.02	0.6±0.3	0.06±0.03
*Chloroflexi**	1.9±0.9	2.4±0.4	2.3±0.6	3.8±1.4	0.6±0.2
Cyanobacteria	44±10.4	32.8±0.9	34±2.6	24.2±5.2	4.4±1.9
*Dependentiae**	0.03±0.02	0.1±0.07	0.1±0.02	0.04±0.01	0.07±0.02
*Firmicutes**	0.18±0.06	0.07±0.02	0.1±0.01	0.06±0.05	0.03±0.01
*Gemmatimonadetes**	0.07±0.004	0.3±0.05	0.36±0.09	0.14±0.03	1.3±0.63
*Hydrogenedentes**	0.09±0.06	0.04±0.02	0.04±0.02	0.01±0.007	0.01±0.002
*Omnitrophicaeota**	0.01±0.01	0.06±0.04	0.06±0.02	0.01±0.002	0.01±0.01
Planctomycetes	13.9±2.42	14.3±1.58	13.2±2.03	18.6±2.23	5.7±1.97
Proteobacteria	11.4±0.92	11.8±0.78	13.3±1.13	12.4±2.62	23.8±4.56
*Spirochaetes**	0.01±0.007	0.15±0.06	0.15±0.05	0.15±0.01	0.17±0.01
Verrucomicrobia	13.5±7.9	18.4±0.9	17.6±0.9	23.6±0.7	17.3±3.3

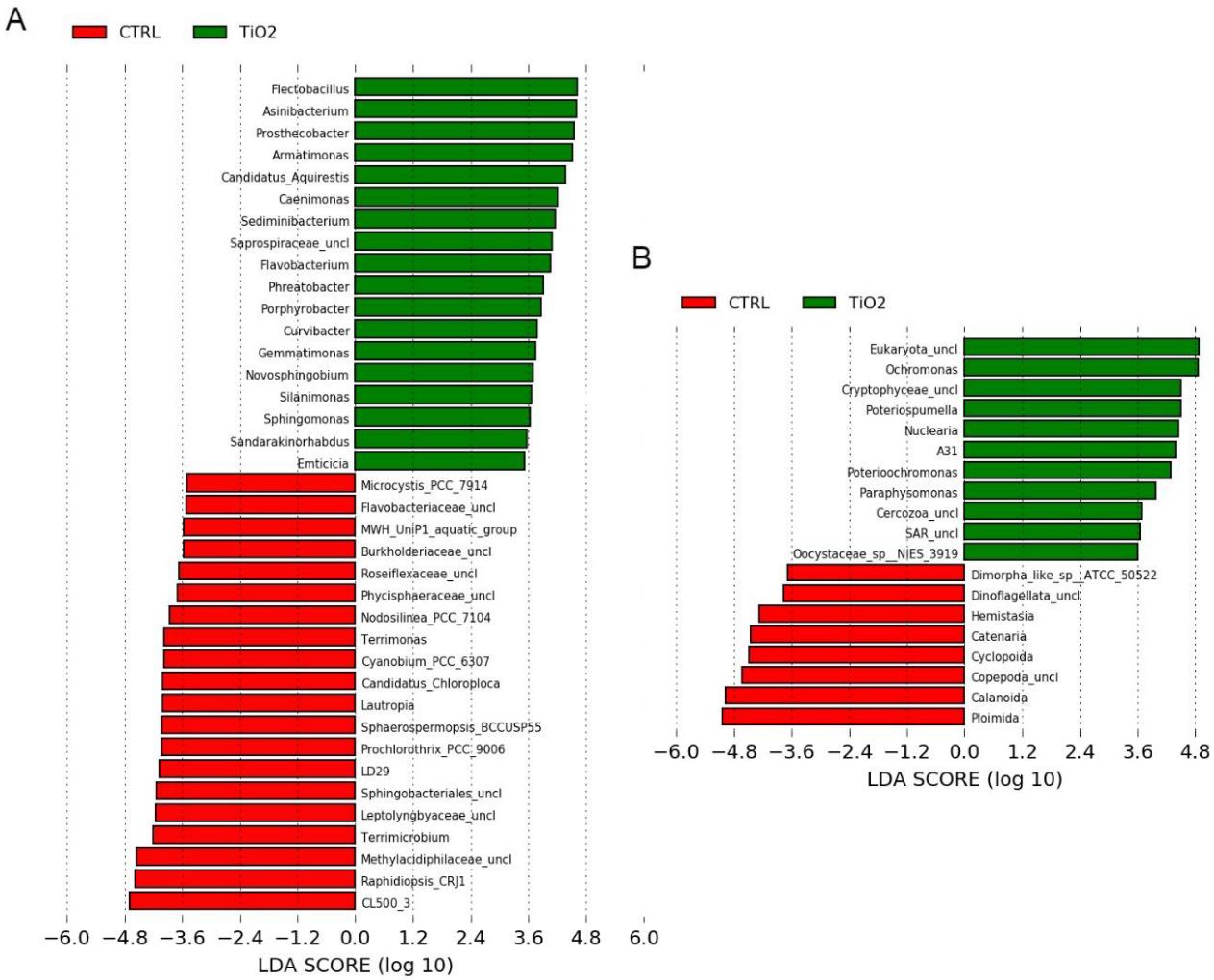

Figure S2: Linear discriminant analysis coupled to effect size (LEfSe) of bacterial (A) and eukaryotic (B) plankton communities considering abundance of the main taxa in treatment and control at day 7. Taxa with significantly different distribution between treatment (TiO_2) and control groups were selected using a p-value < 0.05 and a LDA score (log10) > 3.5.

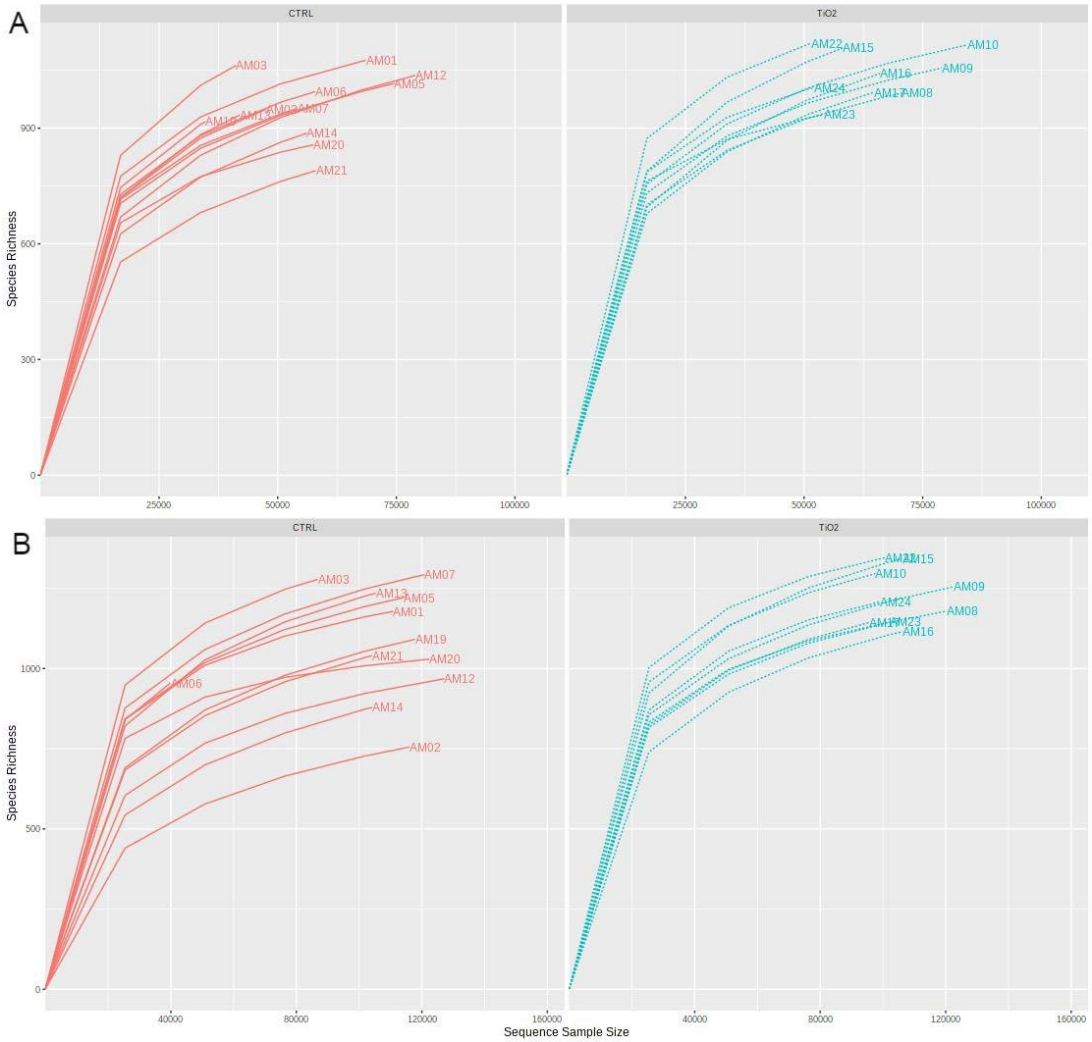

Figure S3: Rarefaction curve of samples from 16 rRNA (A) and 18S rRNA (B) amplicon sequencing indicating the sequencing coverage estimated from the number of species (ASVs). Samples from TiO_2-treatment (green) or control (red).

Table S5: Sample identification, sequencing data and diversity indices for 16S and 18S information. The red line for the AM06 sample (from 18S) means this sample was considered an outlier due the very low sequences number compared to others.

Sample	Description	DNA concentration (ng μL^{-1})	Number of sequences		Goods	Richness	Diversity
			Before trim qual	After trim qual		Sobs	Shannon (H')
16S sequencing information							
AM01	T0	365.2	68595	34791	99.69386	1096	4.688125
AM02	T0	380.35	47565	34791	99.51014	978	4.839721
AM03	T0	329.64	41260	34791	99.35046	1074	4.770999
AM05	No TiO_2 (T3)	183.98	74505	34791	99.71009	1016	4.857933
AM06	No TiO_2 (T3)	158.19	57948	34791	99.62898	1008	4.836678
AM07	No TiO_2 (T3)	420.96	54241	34791	99.60178	966	4.827779
AM08	TiO_2 (T3)	290.99	70512	34791	99.70218	1008	4.787438
AM09	TiO_2 (T3)	199.59	79037	34791	99.71785	1083	4.773695
AM10	TiO_2 (T3)	223.54	84463	34791	99.73716	1131	4.909822
AM12	No TiO_2 (T7)	550.73	79012	34791	99.65955	1060	4.675476
AM13	No TiO_2 (T7)	210.94	41995	34791	99.41183	951	4.695779
AM14	No TiO_2 (T7)	202.42	56182	34791	99.57104	909	4.665011
AM15	TiO_2 (T7)	206.89	58239	34791	99.51407	1137	4.758776
AM16	TiO_2 (T7)	180.4	66043	34791	99.57906	1062	4.489167
AM17	TiO_2 (T7)	339.97	64669	34791	99.60723	1015	4.470062
	18S sequencing information						
AM01	T0	365.2	110933	87335	99.82242	1195	4.130155
AM02	T0	380.35	116267	87335	99.8168	760	1.522841
AM03	T0	329.64	87335	87335	99.72978	1311	4.647847
AM05	No TiO_2 (T3)	183.98	114505	87335	99.78604	1225	4.193731
AM06	No TiO_2 (T3)	158.19	39861	xx	99.35024	955	3.943944
AM07	No TiO_2 (T3)	420.96	120900	87335	99.78577	1296	4.562986
AM08	TiO_2 (T3)	290.99	120383	87335	99.83054	1181	3.872202
AM09	TiO_2 (T3)	199.59	122645	87335	99.80431	1260	4.143498
AM10	TiO_2 (T3)	223.54	97579	87335	99.752	1303	5.213536
AM12	No TiO_2 (T7)	550.73	127122	87335	99.83952	972	3.066831

AM13	No TiO_2 (T7)	210.94	105336	87335	99.73798	1243	3.883575
AM14	No TiO_2 (T7)	202.42	104105	87335	99.74641	881	3.2469
AM15	TiO_2 (T7)	206.89	106102	87335	99.73987	1354	4.44185
AM16	TiO_2 (T7)	180.4	106361	87335	99.77811	1123	3.389061
AM17	TiO_2 (T7)	339.97	95848	87335	99.75795	1153	4.165068

159

160

161

162

163

164

165

166

167

168

169

170

171

172

173

174

175

176

177

178

S4 Effect TiO_2-photocatalysis on abiotic factors (water quality)

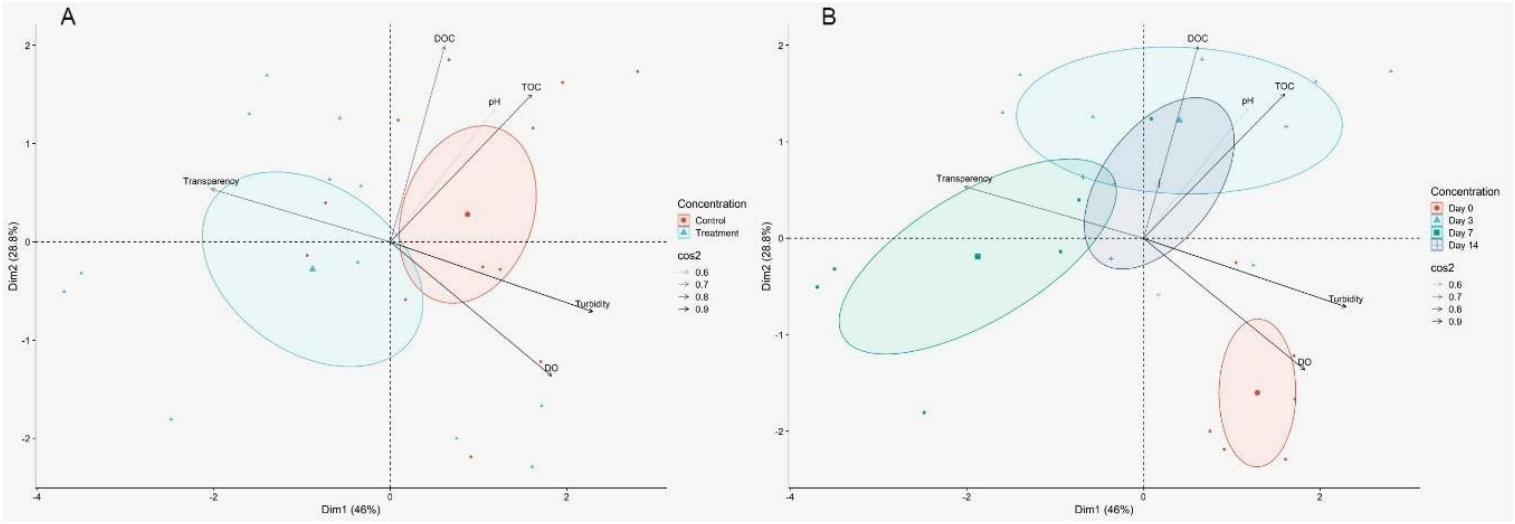

Figure S4: Ordination of the most relevant abiotic parameters considering treatment (A) and time (B) following Principal Component Analysis (PCA) and Ward distance. Both dimensions contributed to explain about 75% of variance of data and the correlation among the parameters.

Table S6: Effect of TiO2-photocatalysis on dissolved nutrient, sulfate, fluoride and chloride content in water. Data are expressed as average and standard deviation (n=3).

	Raw water (T0)	Day 3		Day 7	
		TiO_2	Control	TiO_2	Control
Nitrite (mg L^{-1})	0.77 ± 0.03	0.76 ± 0.01	0.77 ± 0.03	0.77 ± 0.02	0.78 ± 0.02
Nitrate (mg L^{-1})	0.82 ± 0.27	0.42 ± 0.05	0.71 ± 0.04	0.61 ± 0.12	0.62 ± 0.04
Orthophosphate (mg L^{-1})	0.55 ± 0.1	0.93 ± 0.18	0.80 ± 0.12	0.75 ± 0.02	0.67 ± 0.02
Sulfate (mg L^{-1})	4.85 ± 0.34	4.60 ± 0.22	4.47 ±0.32	4.18 ± 0.17	4.60 ± 0.53
Fluoride (mg L^{-1})	2.09 ± 0.32	1.49 ± 0.17	1.58 ±0.26	1.63 ± 0.03	1.72 ± 0.22
Chloride (mg L^{-1})	59.71 ± 2.22	60.69 ± 1.7	60.27 ± 1.65	59.39 ± 0.93	54.64 ± 7.69

S5 Effect of TiO_2-photocatalysis on eukaryotic plankton

Table S7: Relative abundance of eukaryotic community (18S rRNA) from the internal assignment considering defined groups for the freshwater systems from the representative taxa obtained after sequencing. Taxa were chosen using 3% of relative abundance threshold at least in one sample. Data are expressed as mean and standard deviation (n=3) as a percentage of the total eukaryotic community.

Defined groups	Representative taxonomic assignment	T0	Day 3		Day 7	
			Control	TiO_2	Control	TiO_2
Diatom	Bacillariophyceae	1.1 ± 0.8	1.2 ± 0.3	1.4 ± 0.5	0.6 ± 0.3	0.3 ± 0.2
	Fragilariales	9.9 ± 8.2	3.9 ± 1.3	3.6 ± 1.1	5.6 ± 4.2	5.4 ± 3.2
	Mediophyceae	2.1 ± 2.2	1.8 ± 0.3	2.3 ± 0.5	0.8 ± 1	1.5 ± 0.9
Chlorophyta	Chlorophyta	1.6 ± 1.4	1.1 ± 0.1	1.2 ± 0.5	0.4 ± 0.3	0.4 ± 0.2
Zooplankton	Podocopa	2.6 ± 2.7	0 ± 0	1.8 ± 1.9	0 ± 0	0 ± 0
	Gastrotricha	0.8 ± 1.1	0 ± 0	0 ± 0	0.2 ± 0.2	0.3 ± 0.4
	Copepoda	49.9 ± 33.4	38.3 ± 10.9	35 ± 27.3	41.1 ± 14.4	4.6 ± 5.4
	Monogononta	8.3 ± 6	15.3 ± 6.9	13.6 ± 6.2	25.8 ± 13.1	1.7 ± 1
Fungi	Blastocladiales	0.2 ± 0.1	0.5 ± 0.1	0.6 ± 0.3	6.2 ± 2.6	0.1 ± 0.1
Alveolate	Dinoflagellata	4 ± 5.7	0.4 ± 0.1	0.4 ± 0.2	2.4 ± 1	1.1 ± 0.5
	Perkinsidae	1 ± 1	1.1 ± 0.1	1.1 ± 0.1	1.6 ± 1.4	8 ± 3.6
	Hypotrichia	0.6 ± 0.6	1.3 ± 0	2.1 ± 1.6	0.1 ± 0.1	0.4 ± 0.2
	Choreotrichia	0.3 ± 0.3	2.5 ± 0.5	2.8 ± 2	0.4 ± 0.5	0 ± 0
Chrysophyte	Chromulinales	0.5 ± 0.4	0.6 ± 0.1	0.6 ± 0.2	0 ± 0	11.7 ± 2.7
	Chrysophyceae	0.1 ± 0.1	0 ± 0	0 ± 0	0 ± 0	10.2 ± 2.1
	Ochromonadales	0.5 ± 0.6	1.5 ± 0.2	1.6 ± 0.3	0.4 ± 0.6	18.9 ± 11.8
Cryptophyte	Cryptophyceae	3.5 ± 3	2.2 ± 0.3	2.9 ± 2	2.9 ± 2.6	1 ± 0.6
Nucleariids	Nucleariidae	0 ± 0	0.1 ± 0	0.1 ± 0.1	0.1 ± 0	6.6 ± 7.1
Eukaryotic_picoplankton_environmental_sample	Eukaryotic_picoplankton_environmental_sample	0.6 ± 0.5	2 ± 0.1	2.4 ± 1.4	0 ± 0.1	0.2 ±0.1
Discicristata_Euglenid	Discicristata	0.3 ± 0.3	3.3 ± 0.6	3.6 ± 1.2	0.1 ± 0	0.2 ± 0.1
	Prokinetoplastina	0.3 ± 0.3	0.2 ± 0	0.3 ± 0.1	0.3 ± 0.2	0.6 ± 0.3
Unclassified	Incertae_Sedis	0.7 ± 0.4	0.8 ± 0.3	0.7 ± 0.3	4.5 ± 0.4	0.5 ± 0.3
	MAST_12C	0.8 ± 0.6	0.7 ± 0.1	0.8 ± 0.3	0.5 ± 0.1	0.2 ± 0.1
Stramenopiles_uncl	Stramenopiles_uncl	0.7 ± 0.4	1.5 ± 0.2	1.6 ± 0.4	1.1 ± 0.4	2 ± 1.8
SAR_uncl	SAR_uncl	4.1 ± 4.2	2.5 ± 0.3	2.5 ± 0.8	0.6 ± 0.4	1.7 ± 0.5
Eukaryota_uncl	Eukaryota_uncl	5.3 ± 3	17.2 ± 1.9	17.1 ± 6.9	4.2 ± 1.3	22.4 ± 1.7

S6 Correlation between plankton and abiotic factors during TiO_2-photocatalysis

Table S8: Spearman correlation between the main genera, which contributed to the difference between control and treatment according to LEfSe analysis, with physical chemical parameters that showed a difference over the treatment. Spearman r values (threshold r=0.4) are labeled considering a negative (in red) or positive (in green) correlation, from a significant p-value (p<0.05).

Bacterioplankton						
Spearman (p<0.05)	**Dissolved O_2**	**pH**	**Turbidity**	**Transparency**	**TOC**	**DOC**
Armatimonas	-	-	-	-	-	-
Asinibacterium	-0.5472		-0.73847	0.56965	-	-
CL500_3	-	-	-	-	-0.4663	-
Cyanobium	-	-	0.52406	-0.60417	-0.4487	-
Flectobacillus	-	-0.5104	-	-	-	-
LD29	-	-	-	-	-0.5828	-
*Leptolyngbyaceae*_uncl	-	0.68182	-	-	-	-
*Methylacidiphilaceae*_uncl	-	-	-	-	-	-
Microcystis	0.50649	-	0.6723	-0.61068	-	-0.5301
Nodosilinea	-	-	0.53966	-0.65886	-	-
Planktothrix	0.4974	-	0.6697	-	-	-
Prochlorothrix	-	0.50341	0.43447	-	-	-
Prosthecobacter	-0.4639	-	-0.44893	0.44104	0.61258	0.49201
Raphidiopsis	-	0.44156	0.54096	-	-	-
Sphaerospermopsis	0.53329	-	0.54504	-	-	-
Terrimicrobium	-	-	-	-	-	-
Eukaryotes						
Spearman (p<0.05)	**Dissolved O_2**	**pH**	**Turbidity**	**Transparency**	**TOC**	**DOC**
Ploimida	-	-	-	-	-	-
Calanoida	-	-	0.48795	-	-	-0.5324
Copepoda_uncl	-	-	-	-	-	-
Cyclopoida	-	-	-	-0.54388	-0.4464	-
Catenaria	-	-	-	-	-	-
Ochromonas	-	-	-	0.57703	0.46833	0.58158
*Cryptophyceae*_uncl	-	-	-	-	-	0.47281
Poteriospumella	-	-	-0.44646	-	-	-
Nuclearia	-0.4947	-	-0.63102	0.55066	0.55506	0.53022

S7 Stability of TiO_2 coating and post-deployment photocatalytic performance of coated glass beads

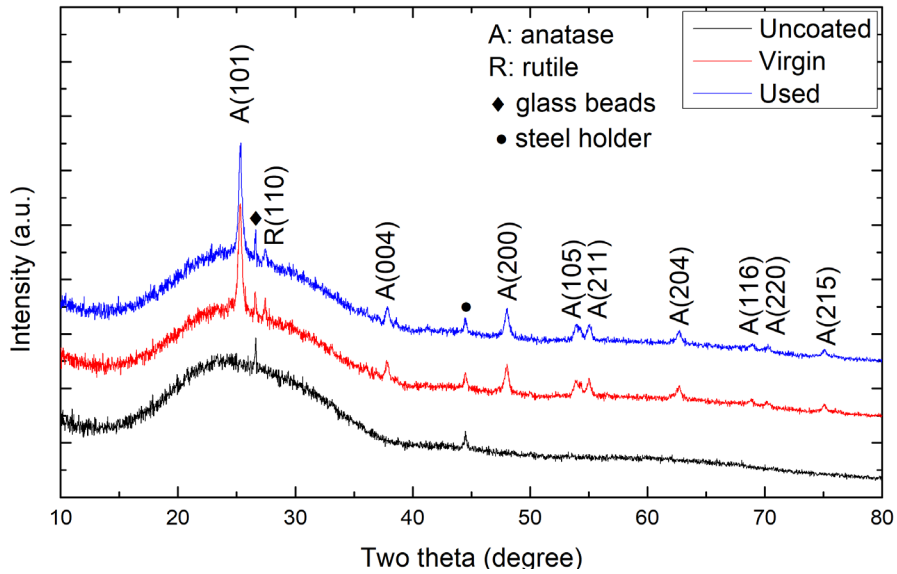

213

214 **Figure S5:** XRD analysis of uncoated, virgin, and used glass beads made from post-

215 consumer glass and coated with TiO_2 (virgin and used) showing the stability of the TiO_2-

216 coating on the beads.

217

Virgin beads

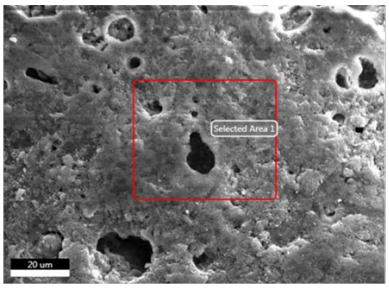

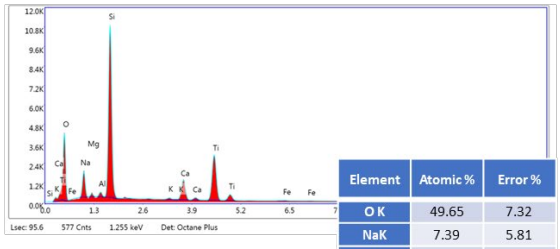

Element	Atomic %	Error %
O K	49.65	7.32
Na K	7.39	5.81
Mg K	0.60	11.23
Al K	0.73	7.59
Si K	25.31	2.20
K K	0.28	18.67
Ca K	4.43	2.94
Ti K	11.45	1.83
Fe K	0.15	62.33

Used beads

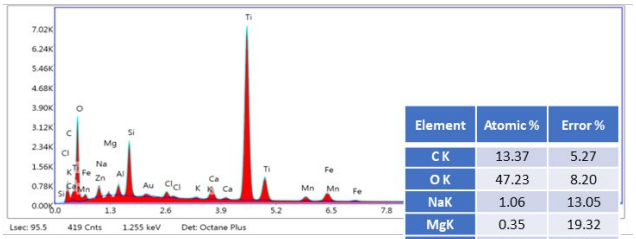

Element	Atomic %	Error %
C K	13.37	5.27
O K	47.23	8.20
Na K	1.06	13.05
Mg K	0.35	19.32
Al K	1.07	7.07
Si K	5.02	3.41
Au M	0.09	23.56
Cl K	0.60	13.27
K K	0.21	21.41
Ca K	1.60	4.97
Ti K	25.49	1.70
Mn K	0.92	11.21
Fe K	2.06	6.28
Zn K	0.93	14.25

218

Figure S6: SEM and EDS analysis of virgin and used TiO_2-coated glass beads made from post-consumer glass showing the incorporation of Fe and Mn (from reactor components into the elemental composition) and showing stability of coating.

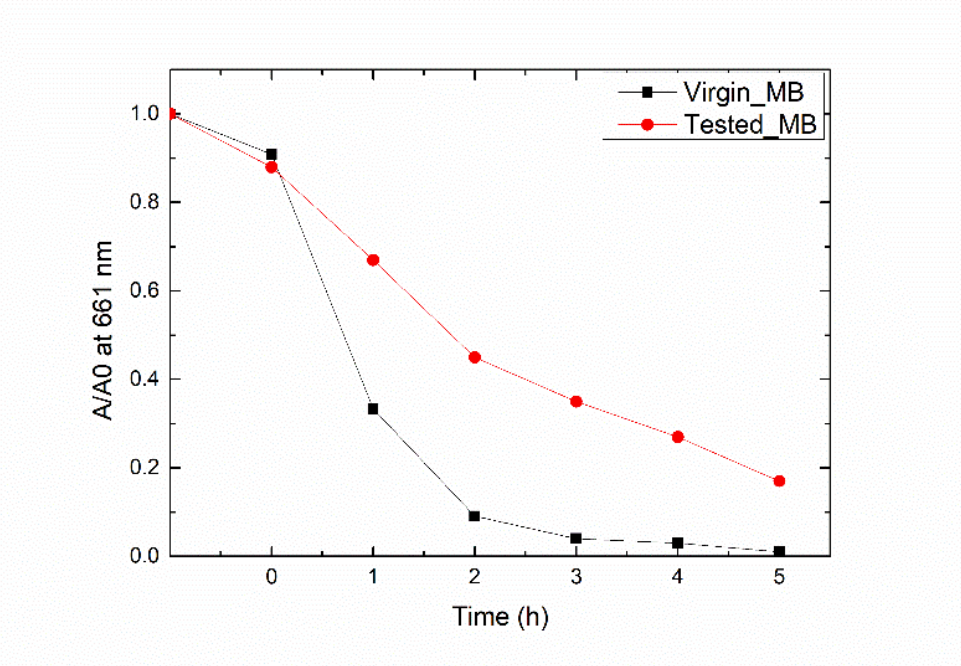

Figure S7: Removal of methylene blue by virgin and used (tested) TiO2-coated glass beads made from post-consumer glass using a 250 W iron doped metal halide lamp (λ > 250 nm) at room temperature.

S8 Preliminary cost analysis of the proposed TiO_2-photocatalytic treatment system

Estimation of the cost of a prototype treatment unit is difficult and can be, at best, preliminary. As with any process engineering application cost will need to be determined on a case by case basis. As detailed in the manuscript one of the principles of the *in-situ* concept is that it will be operated over specific periods or continuously to lower the load of cyanobacteria that a water treatment plant will

ultimately need to remove prior to distribution onto the network. As with any process design the overall cost of the process will comprise:

- capital costs,
- fixed costs,
- variable costs,
- operations and maintenance costs.

For this unit the capital/fixed costs will include the cost of the individual treatment pods which comprise the mesh for the unit housing, LED strips and photocatalyst immobilised on the glass beads. As described in the paper the in-situ unit will comprise arrays of these pods depending on the scale of process so the fixed cost of the treatment pods will be dictated by how pods are required. In this study the overall cost for each treatment unit was approximately USD 630 broken down into ~USD 565 for 5 m of water-proof (IP68) 365 nm LED strips with 120 LEDs m^{-1}, ~USD 27 for 0.5 m^2 of the stainless steel wire mesh to construct the housing and the pods, and an additional ~USD 30 for the aluminium profiles that anchor the LED strips inside of the reactor shell and the water-proof wiring. The raw material cost for the TiO_2-coated beads is ~USD 3 for the quantity of beads required for a single reactor.

Again, as detailed in the manuscript, the units may be powered by floating photovoltaic units and this is the other substantial capital cost. The costs of the platform will include costs for:

- Photovoltaic Solar Panels
- Floats to support the PV Panels

- Moorings
- Electrical Cables between panels and to the LEDs in the reactor pods

As the LED arrays use DC there is no requirement for an inverter for this system. In terms of costs of power generated from the floating photovoltaic systems the overall cost per kWh of commercial floating photocaltaic systems are estimated as being between 0.05-0.07 $ kWh. The operational and maintenance costs will again depend on each system and for water treatment systems can vary between 15 and 40% of the overall annual costs and are influenced by a variety of factors such as the scale of the unit.

References

Cavalier-Smith, T., 2018. Kingdom Chromista and its eight phyla: a new synthesis emphasising periplastid protein targeting, cytoskeletal and periplastid evolution, and ancient divergences. Protoplasma 255, 297–357. https://doi.org/10.1007/s00709-017-1147-3

Riba, M., Kiss-Szikszai, A., Gonda, S., Parizsa, P., Deak, B., Torok, P., Valko, O., Felfoldi, T., Vasas, G., 2020. Chemotyping of terrestrial *Nostoc* like isolates from alkali grassland area s by non targeted peptide analysis. Algal Res. 46, 101798. https://doi.org/https://doi.org/10.1016/j.algal.2020.101798

Savegnago, R.P., Caetano, S.L., Ramos, S.B., Nascimento, G.B., Schmidt, G.S., Ledur, M.C., Munari, D.P., 2011. Estimates of genetic parameters, and cluster and principal components analyses of breeding values related to egg production traits in a white leghorn population. Poult. Sci. 90, 2174–2188. https://doi.org/10.3382/ps.2011-01474

Segata, N., Izard, J., Waldron, L., Gevers, D., Miropolsky, L., Garrett, W.S., Huttenhower, C., 2011. Metagenomic biomarker discovery and explanation. Genome Biol. 12, 1–18. https://doi.org/10.1186/GB-2011-12-6-R60/FIGURES/6

Simpson, A.G.B., Eglit, Y., 2016. Protist diversification, in: Kliman, R.M. (Ed.), Encyclopedia of Evolutionary Biology Volume 3. Elsevier, Amsterdam, pp. 344–360.

Vaissie, P., Monge, A., Hudsson, F., 2020. Fac toshiny: Perform Factorial Analysis from "FactoMineR" with a Shiny Application. R-package version 2.2.